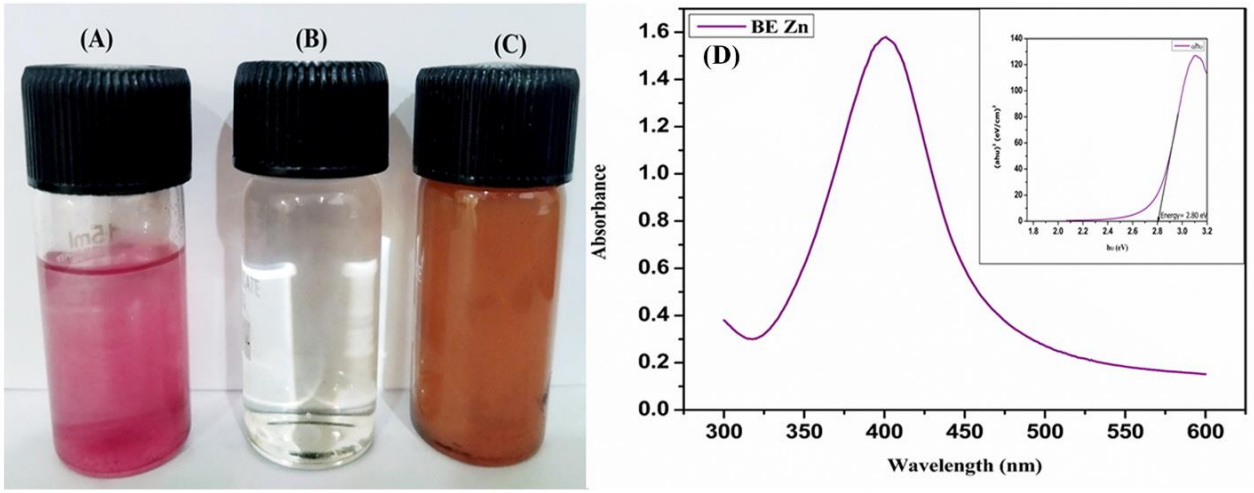

Fig.1. (A) 1 mM betanin, (B) 0.1 M of Zinc nitrate Solution, (C) Synthesized BE-ZnO-NPs (D) UV analysis of BE-ZnO-NPs.

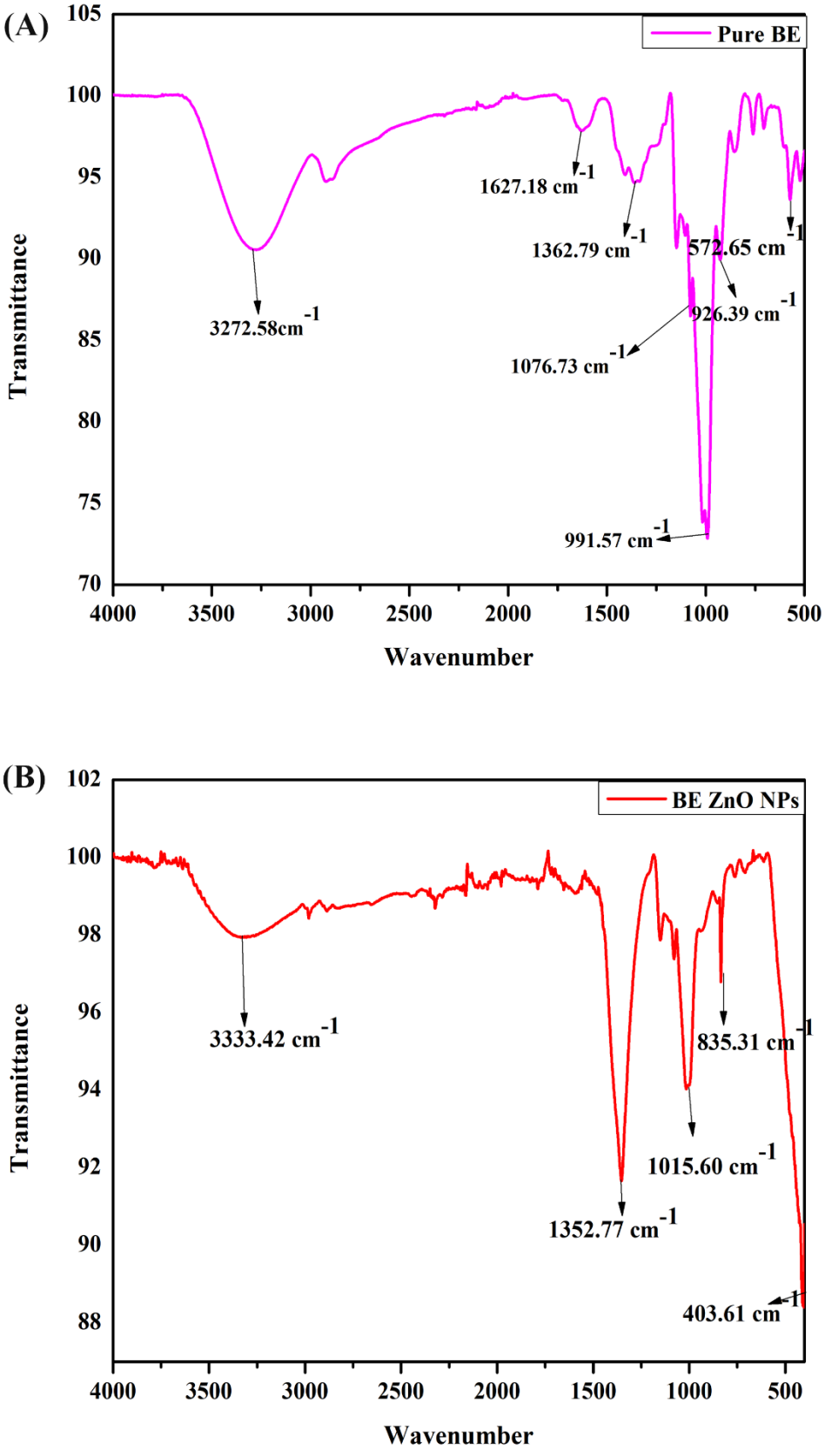

Fig.2. FTIR analysis for: (A) Pure Betanin. (B) BE mediated ZnO-NPs.

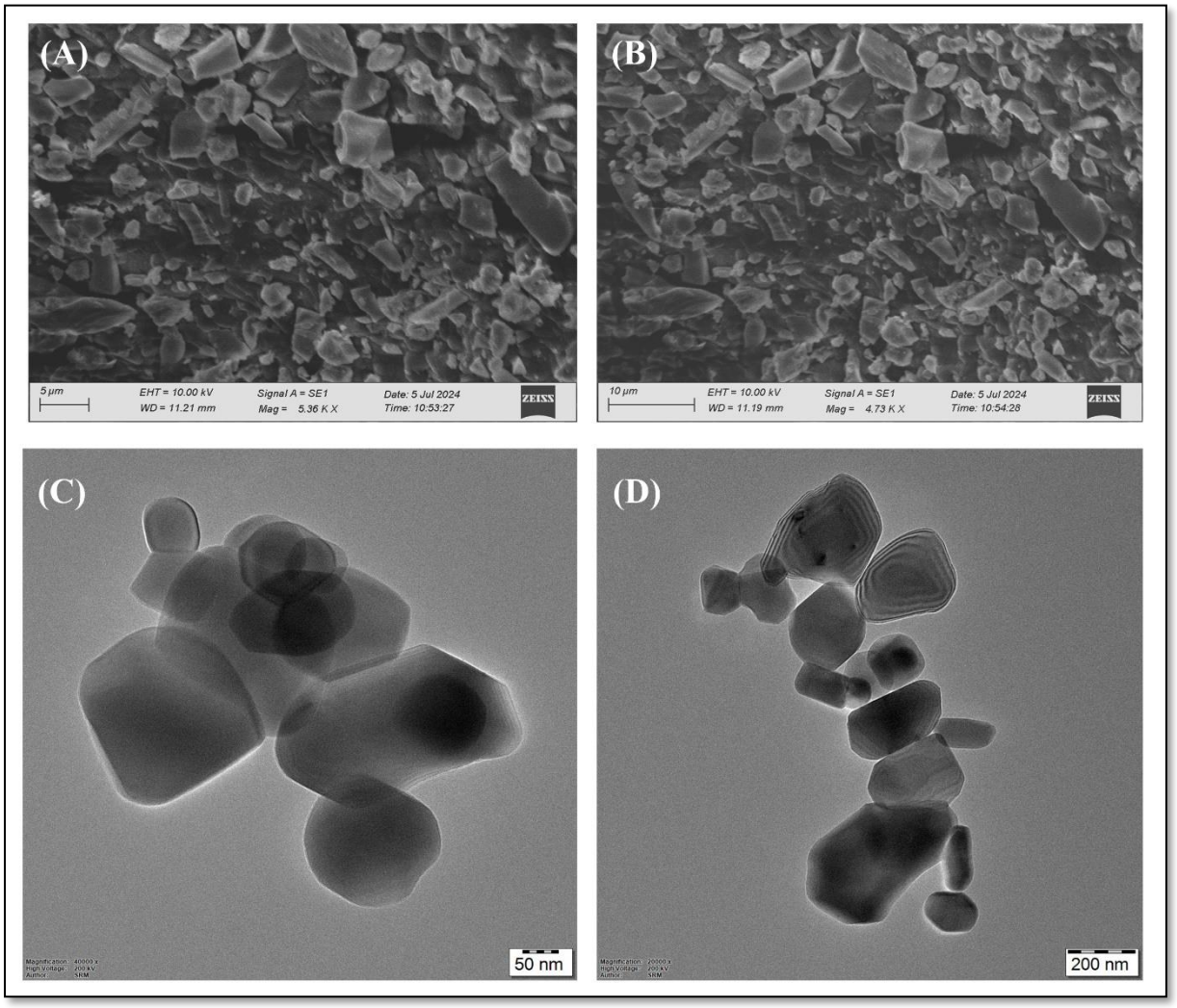

Fig.3. (A) and (B) represent SEM images of BE-ZnO-NPs, (C) and (D) represent TEM images.

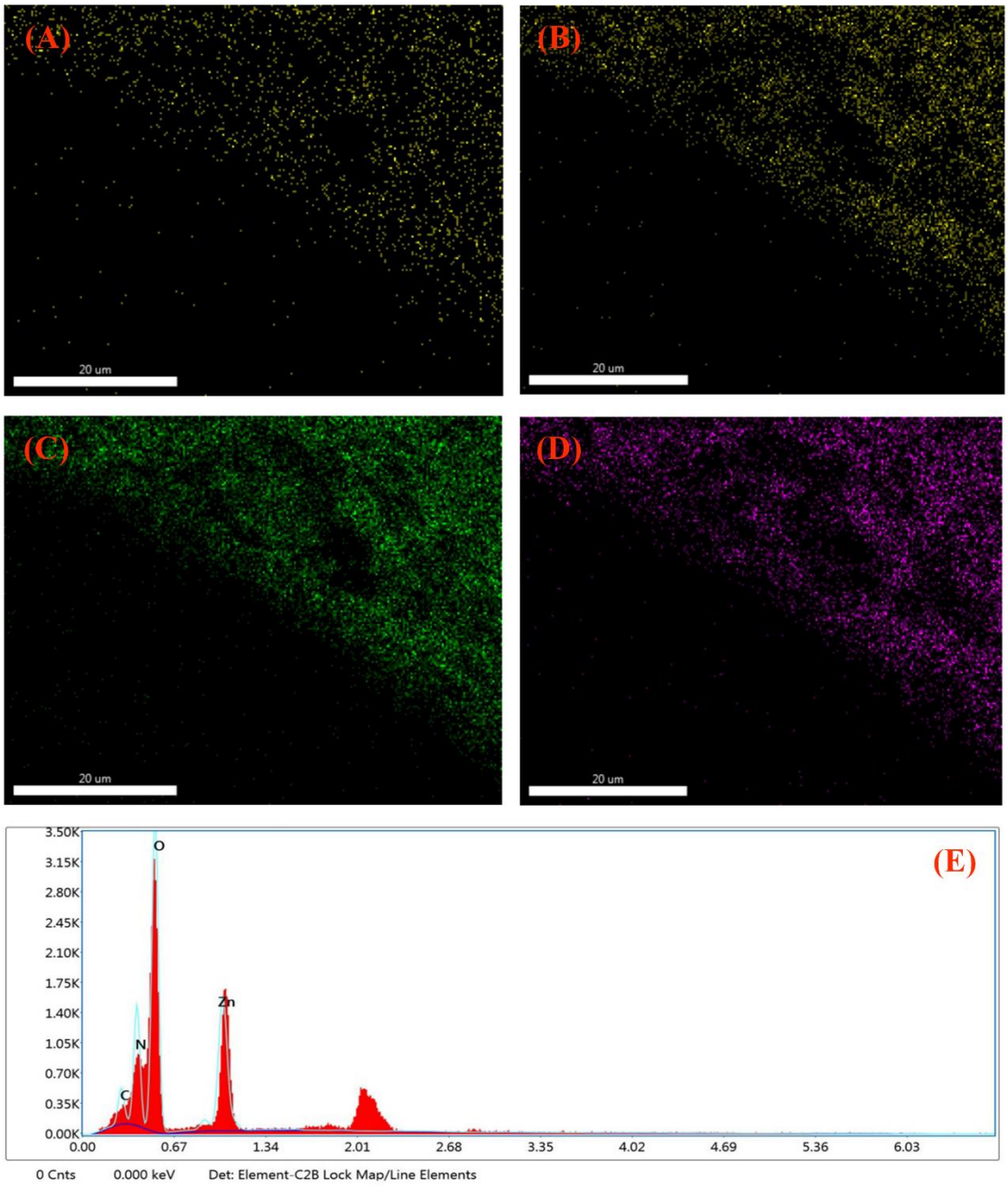

Fig.4. EDX colour mapping: (A) Carbon, (B) Nitrogen, (C) Oxygen and (D) Zinc and (E) EDX spectrum of BE mediated ZnO-NPs.

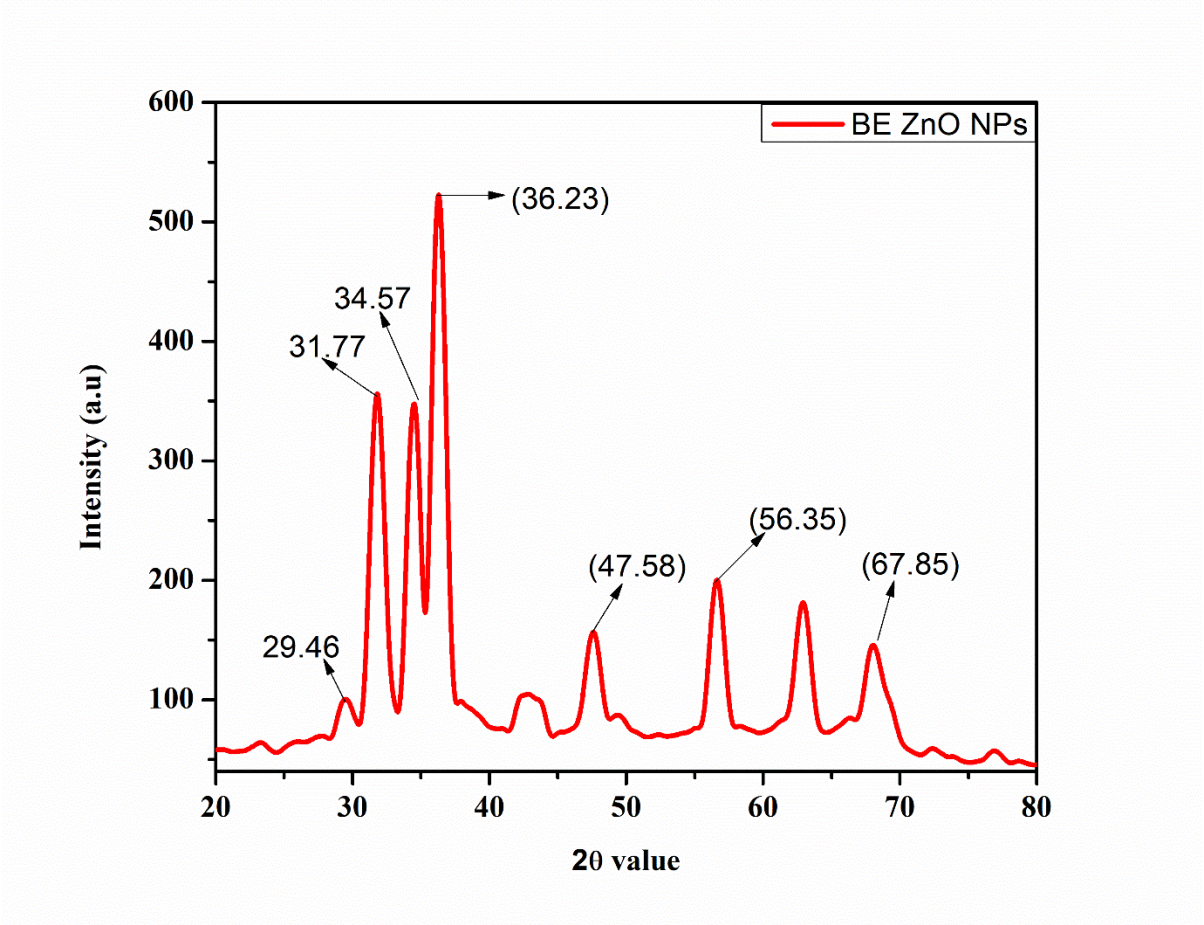

Fig.5. X-ray Diffraction spectrum of BE-ZnO-NPs.

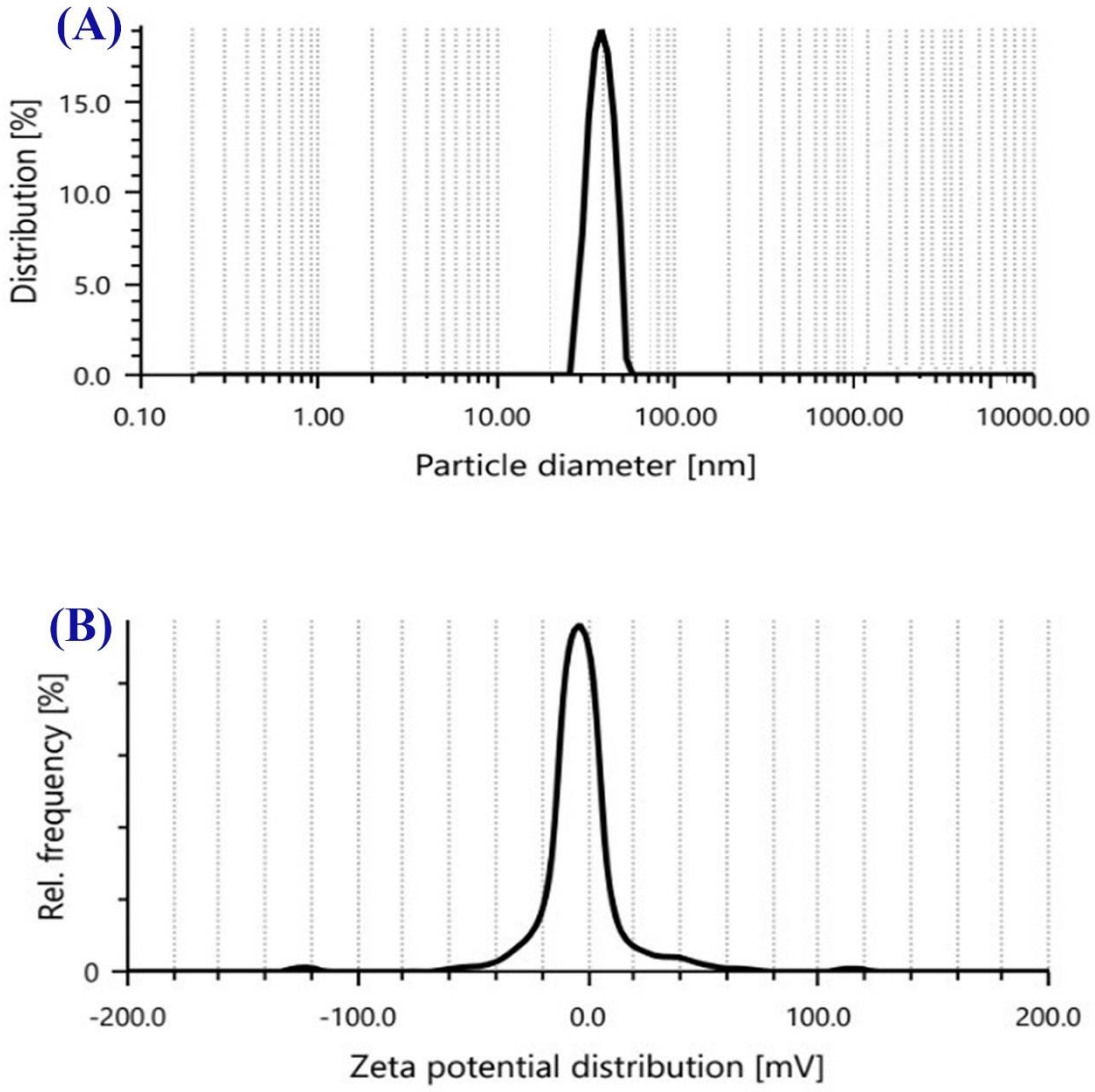

Fig.6. (A) DLS particle size of BE-ZnO-NPs and (B) Zeta potential of BE-ZnO-NPs.

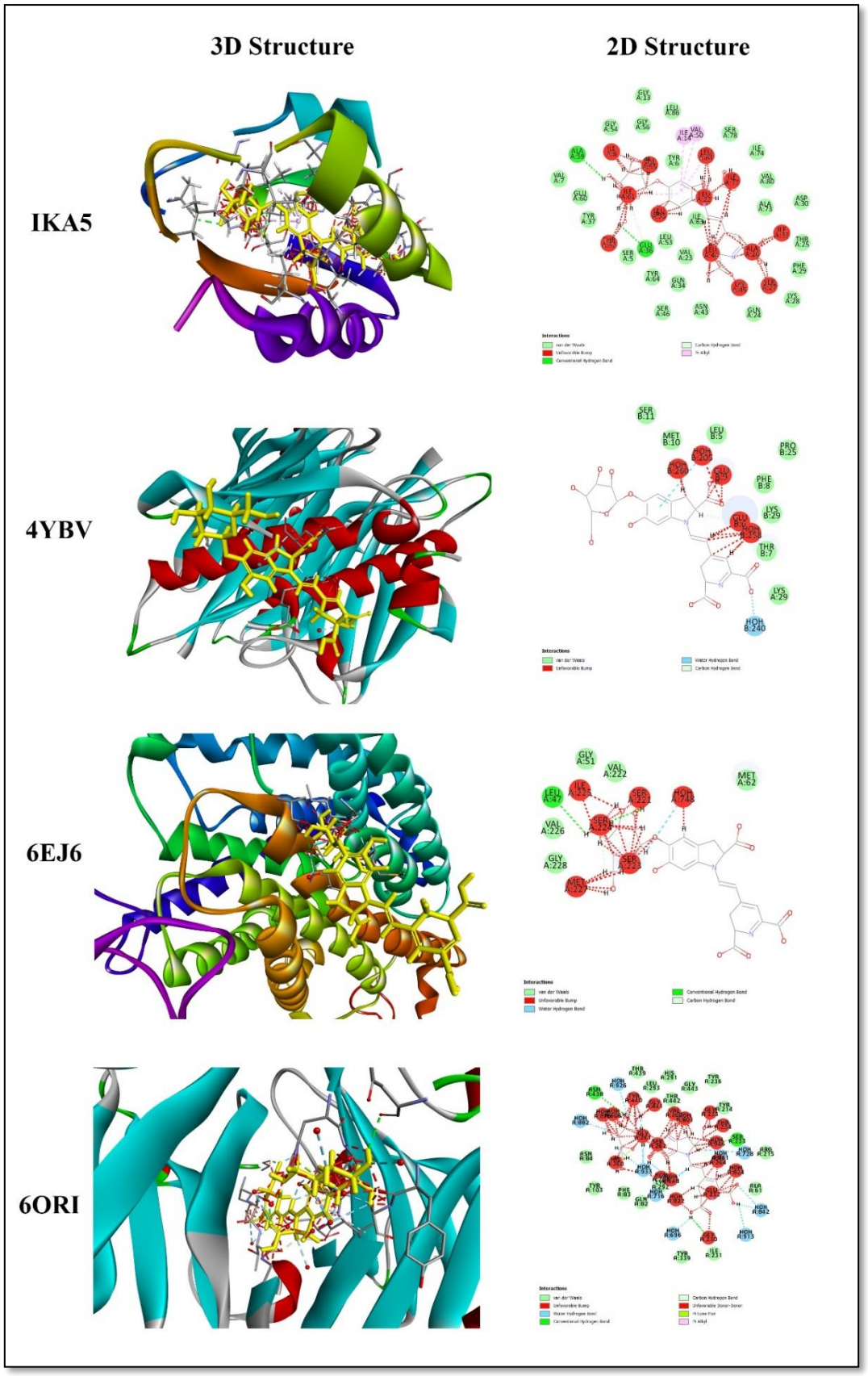

Fig.7. 3D and 2D representative images of BE and dental pathogen receptor interactions. Receptor-IKA5 (*S. aureus*), 4YBV (*S. mutans*), 6EJ6 (*C. albicans*) and 6ORI (*E. faecalis*).

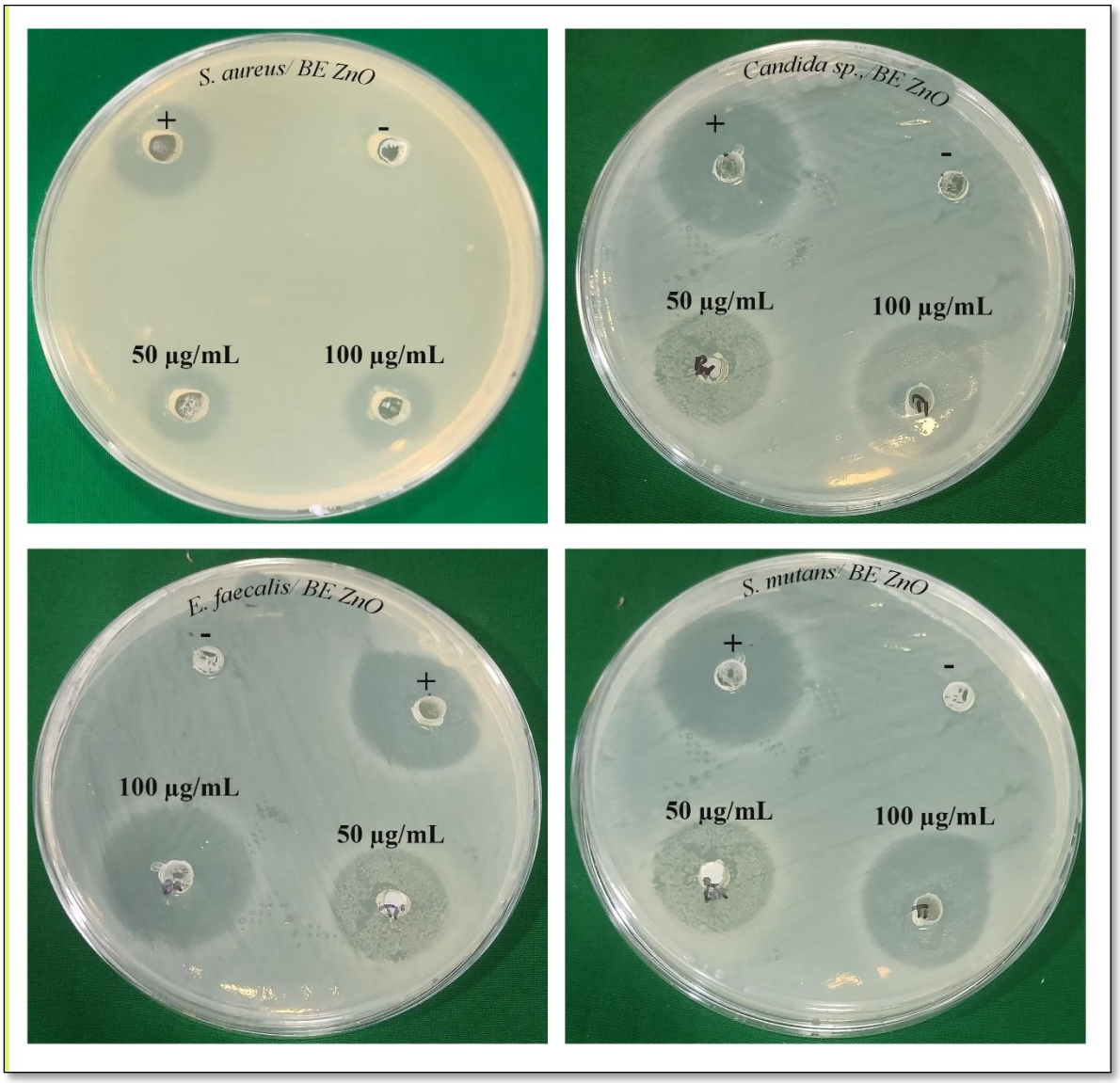

Fig. 8. Antimicrobial activity of BE-ZnO-NPs against dental pathogens (well diffusion method) using strains: *S. aureus, C. albicans, S. mutans*, and *E. faecalis*. "+" indicates-positive control-Amoxicillin 5µg/mL).

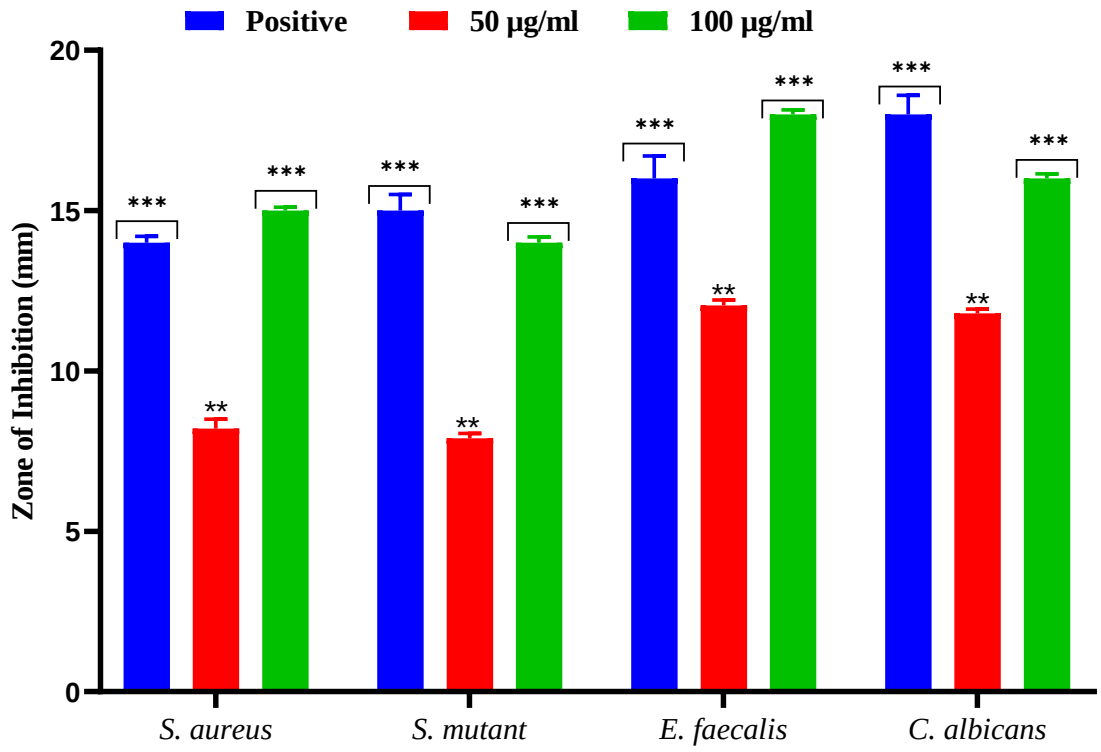

Fig.9. Zone of inhibition (well diffusion method) of BE-ZnO-NPs was evaluated against dental pathogens including *S. aureus, S. mutans, E. faecalis*, and *C. albicans* at various concentrations. Amoxicillin served as the positive control (5 µg/ml). The asterisk (*) denotes statistical significance (**$p<0.005$) and (***$p<0.0005$) compared to the control. Results are expressed as the mean ± standard deviation from three distinct experiments.

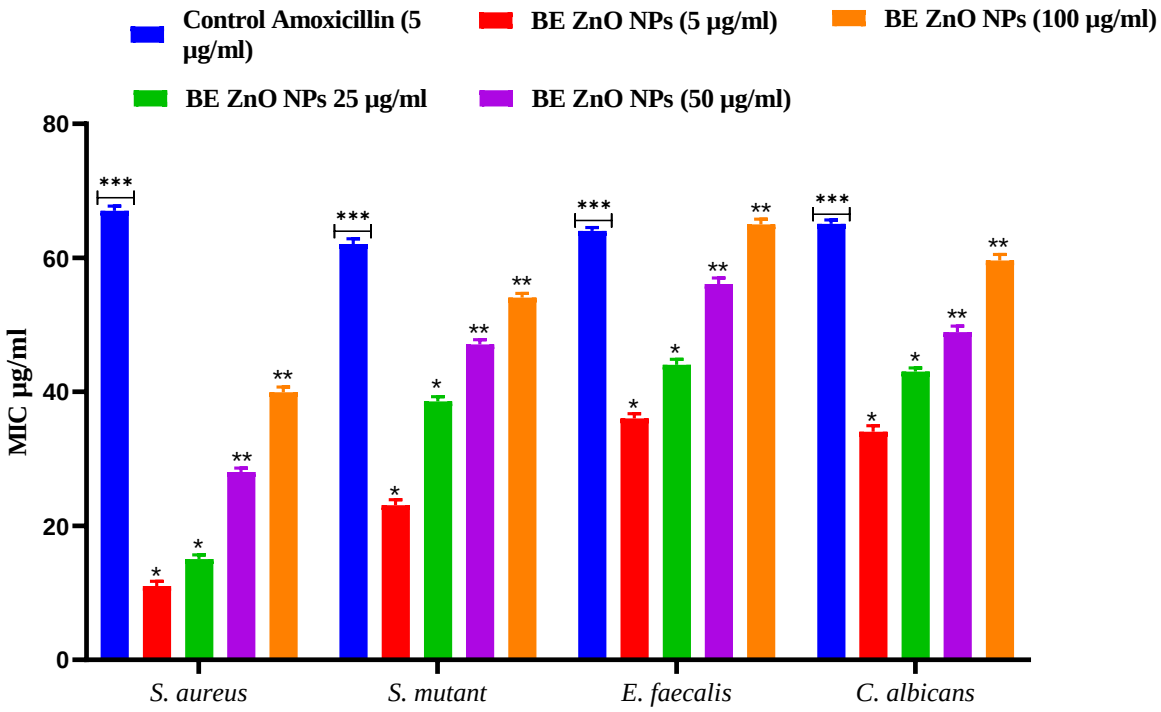

Fig.10. The MIC of BE-ZnO-NPs was evaluated against dental pathogens including *S. aureus*, *S. mutans, E. faecalis, and C. albicans* at various concentrations. Amoxicillin served as the positive control. The asterisk (*) denotes statistical significance (*p<0.05), (**p<0.005) and (***p<0.0005) compared to the control. Results are expressed as the mean ± standard deviation from three distinct experiments

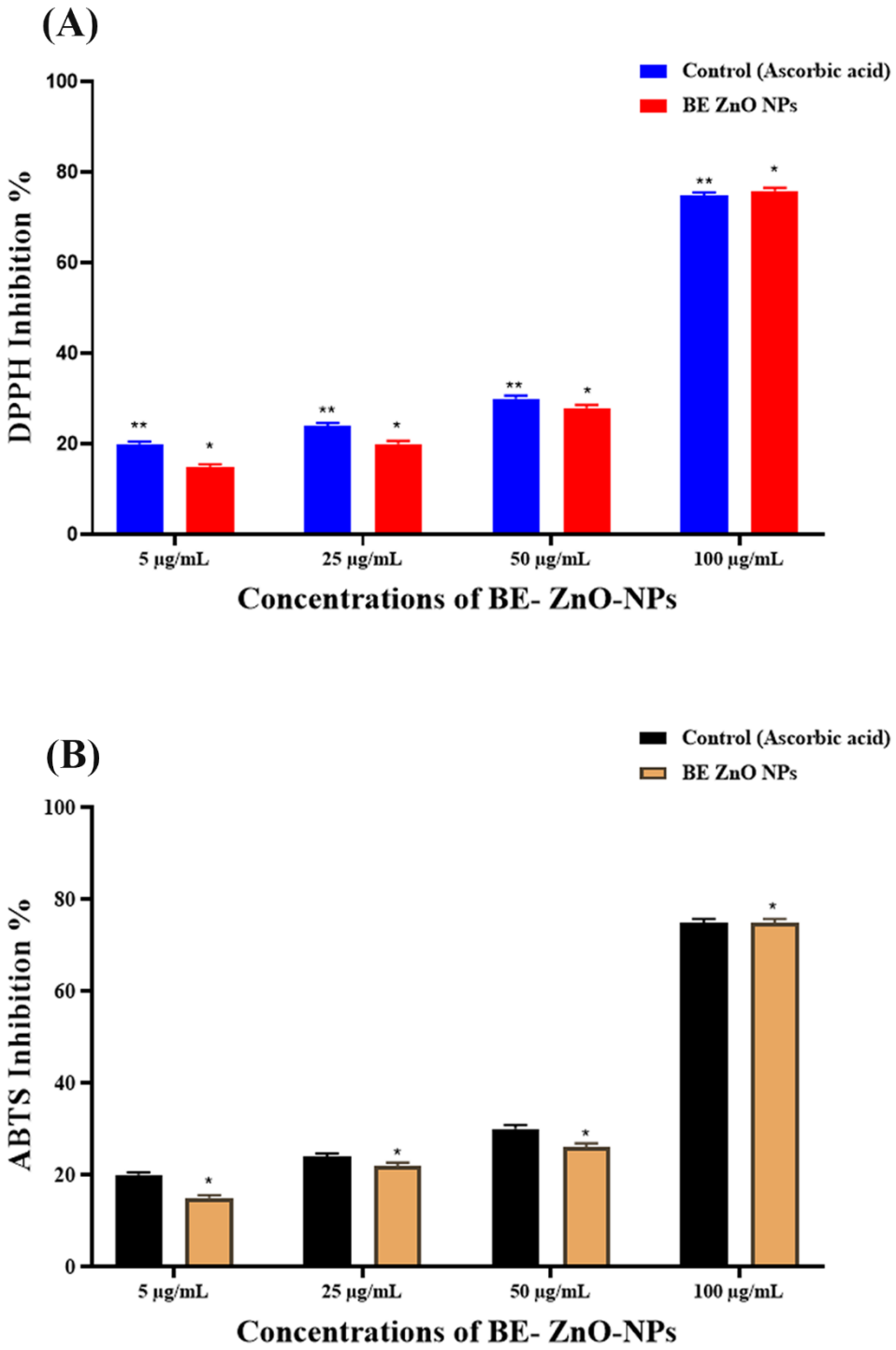

Fig. 11. Antioxidant potential of BE-ZnO-NPs were assessed at various concentration (A) DPPH assay. (B) ABTS scavenging activity. The (*) Asterisk denotes statistically significant (*$p<0.05$) compared to control (Ascorbic acid).

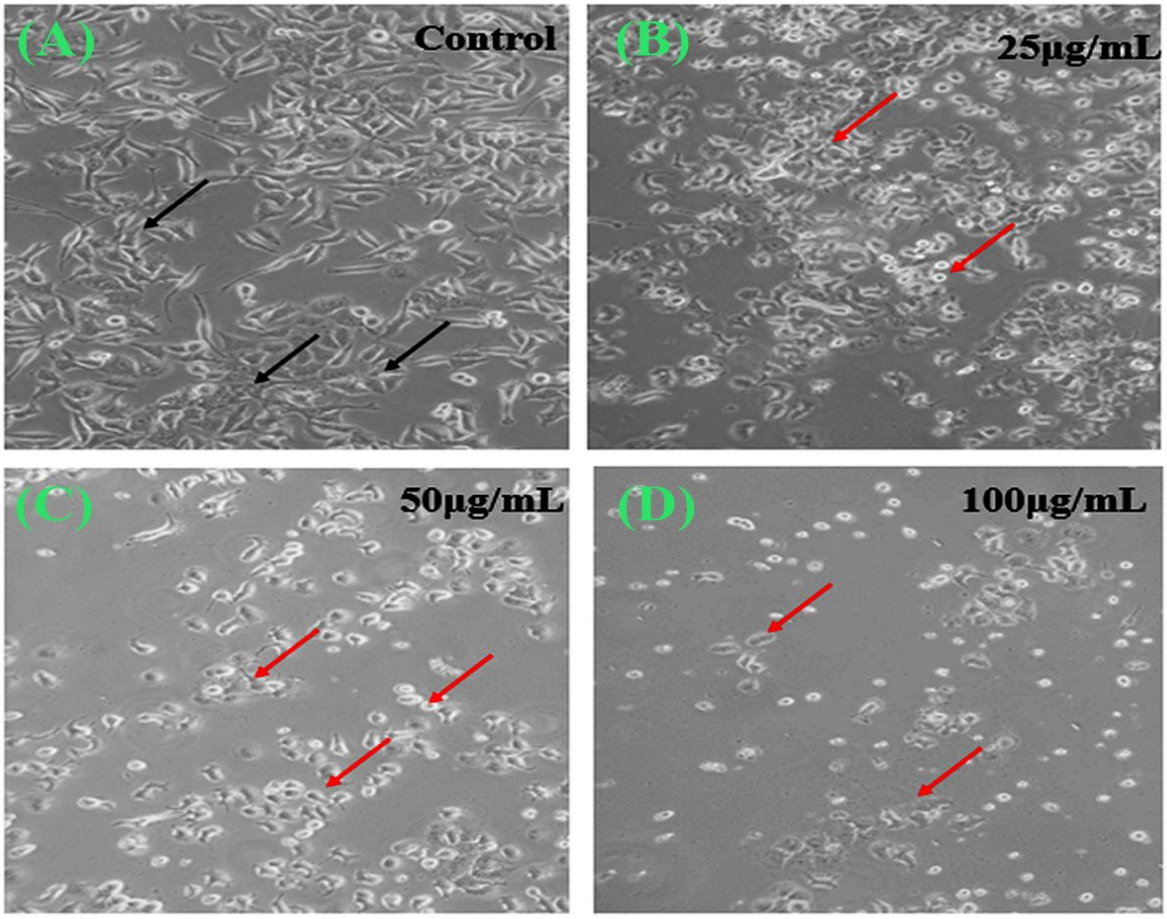

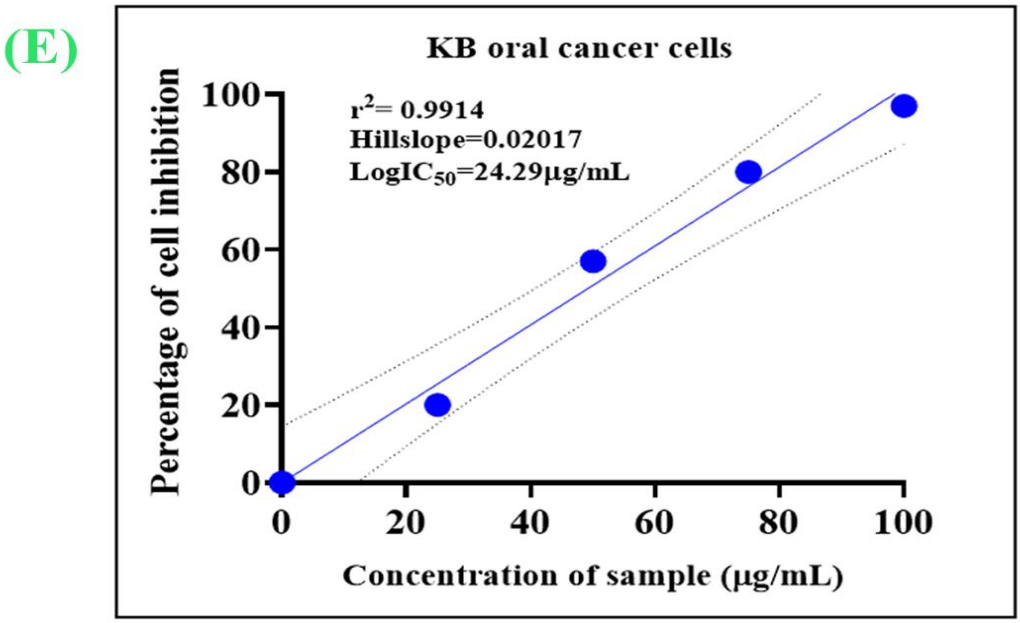

Fig.12. MTT assay of BE-ZnO-NPs against KB cells: (A) Black arrow indicates healthy cells in control and in (B), (C) & (D) cell treated with various doses of BE-ZnO-NPs reveals cell shrinkage were indicated by red arrow. (E) Percentage of cell inhibition.

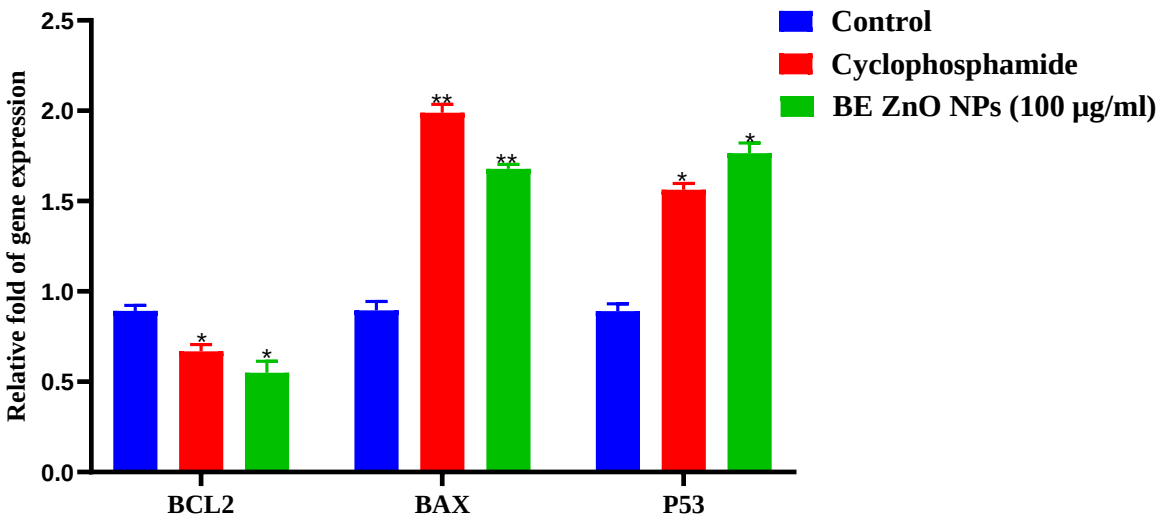

Fig.13. The impact of BE-ZnO-NPs treatment on the mRNA expression levels of BCL2, BAX, and P53 was assessed. Results are presented as the mean ± standard deviation from three separate experiments. Statistical significance (* $p<0.05$) & (** $p<0.005$) indicates a comparison with the control group.

Table. 1. Primers used for gene expression

Gene	Forward primer (5′-3′)	Reverse primer (5′-3′)	References
GAPDH	GCCAAAAGGGTCATCATCTCTGC	GGTCACGAGTCCTTCCACGATAC	[10]
BCL-2	GACGACTTCTCCCGCCGCTAC	CGGTTCAGGTACTCAGTCATCCAC	[10]
BAX	AGGTCTTTTTCCGAGTGGCAG	GCGTCCCAAAGTAGGAGAGGAG	[10]
P53	ACATGACGGAGGTTGTGAGG	TGTGATGATGGTGAGGATGG	[11]

Table.2. Amino acid and Binding affinity value of the protein interaction with different dental pathogen receptors. LYS (Lysine), GLY (Glycine), ALA (Alanine), ARG (Arginine), VAL (Valine), ILE (Isoleucine), SER (Serine), ALA (Alanine), LEU (Leucine), GLU (Glutamate), HOH (Water molecule), MET (Methionine), ASN (Asparagine), THR (Threonine), and HIS (Histidine)

Receptor	Ligand	Binding affinity (Kcal/mol)	Amino acid interaction
IKA5 (*S. aureus*)	Betanin	-7.2	ALA, ILE, VAL, THR,LEU, SER, LYS
4YBV (*S. mutans*)	Betanin	-7.3	GLU, HOH
6EJ6 (*C. albicans*)	Betanin	-6.4	LEU, ILE, SER, HOH, MET
6ORI (*E. faecalis*)	Betanin	-8.0	ASN, HOH, THR, GLY, SER, HIS, VAL, GLU

Table.3. ADMET parameters of betanin.

Physiochemical parameters								
MW	**#Heavy atoms**	**#Aromatic heavy atoms**	**Fraction Csp3**	**#Rotatable bonds**	**#H-bond acceptors**	**#H-bond donors**	**MR**	**TPSA**
550.47 g/mol	39	6	0.42	8	14	8	135.13	247.11 Å

Lipophilicity					
iLOGP	**XLOGP3**	**WLOGP**	**MLOGP**	**Silicos-IT Log P**	**Consensus Log P**
0.86	-1.25	-2.55	-2.51	-2.03	-1.50

Pharmacokinetic parameters								
GI absorption	**BBB permeant**	**Pgp substrate**	**CYP1A2 inhibitor**	**CYP2C19 inhibitor**	**CYP2C9 inhibitor**	**CYP2D6 inhibitor**	**CYP3A4 inhibitor**	**log Kp (cm/s)**
Low	No	No	No	No	No	No	No	-10.55

Drug likeness parameters					
Lipinski #violations	**Ghose #violations**	**Veber #violations**	**Egan #violations**	**Muegge #violations**	**Bioavailability Score**
No	No	No	No	No	0.11

Highlights

- BE-ZnO-NPs absorb in the UV–vis spectrum at a wavelength that is centered at 388 nm.
- BE-ZnO NPs demonstrated significant antibacterial activity against dental pathogen *E. faecalis*.
- BE ZnO NPs exhibited dose-dependent antioxidant activity comparable to ascorbic acid.
- Significant cytotoxic effect on oral cancer KB cells with an IC_{50} value of 24.29 µg/mL.
- BE-ZnO NPs induced apoptosis in KB cells by downregulating BCL2 and upregulating BAX and P53.

Graphical abstract

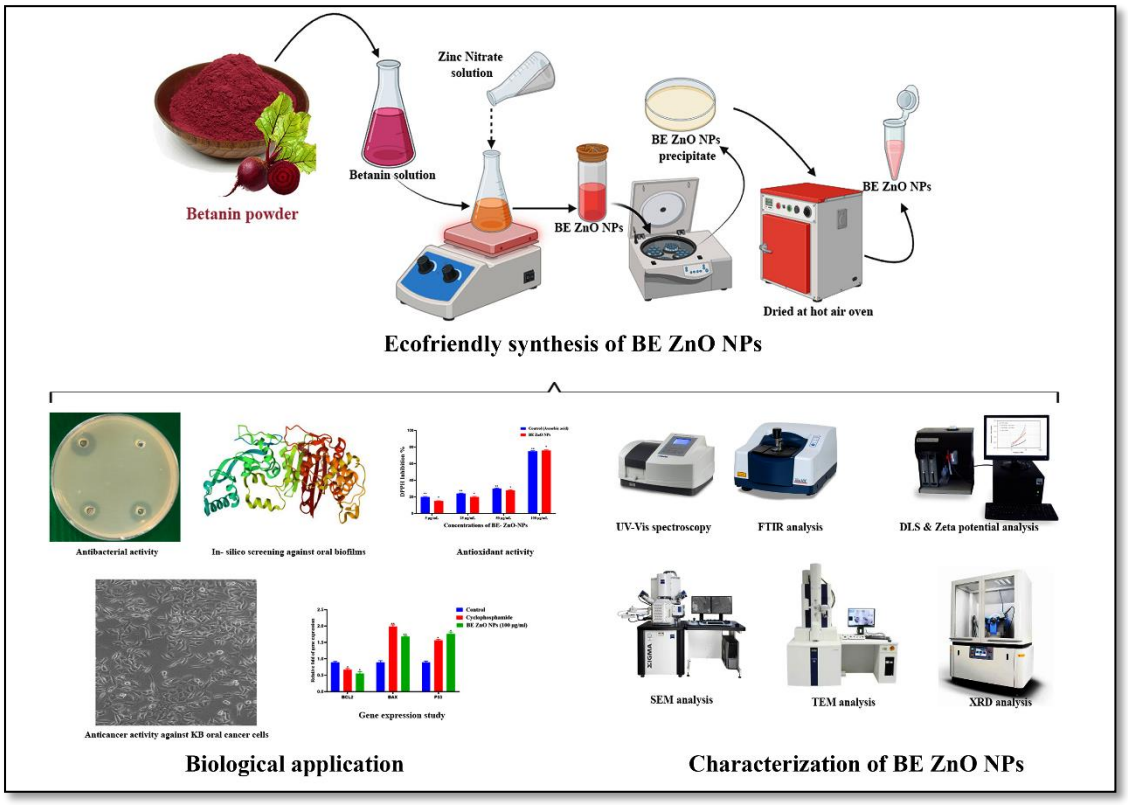

Eco-friendly synthesis of Betanin-conjugated ZnO nanoparticles: Antimicrobial efficacy and apoptotic pathway activation in KB oral cancer cells

Chinnasamy Ragavendran[a], Mohamed Imath[b], Chinnaperumal Kamaraj[c] Ismini Nakouti[4], Salim Manoharadas[5]

[a]Department of Cariology, Saveetha Dental College and Hospitals, Saveetha Institute of Medical and Technical Sciences (SIMATS), Saveetha University, Chennai, India.

[b]Department of Pharmacology, The Tamil Nadu Dr M G R Medical University, Guindy, Chennai, Tamil Nadu, India.

[c]Interdisciplinary Institute of Indian System of Medicine (IIISM), Directorate of Research and Virtual Education, SRM Institute of Science and Technology (SRMIST), Kattankulathur, Chennai-603203, Tamil Nadu, India. E. mail: mullaikamaraj@gmail.com.

[4]Centre for Natural Products Discovery (CNPD), School of Pharmacy and Biomolecular Sciences, Liverpool John Moores University, Liverpool L3 3AF, UK.

[5]Department of Botany and Microbiology, College of Science, King Saud University, P.O. Box. 2454, 11451 Riyadh, Saudi Arabia.

Corresponding author:

#Dr. Chinnasamy Ragavendran. [a]Department of Cariology, Saveetha Dental College and Hospitals, Saveetha Institute of Medical and Technical Sciences (SIMATS), Saveetha University, Chennai-600 077, India. **E. mail**: ragavan889@gmail.com/ ragavendranc.sdc@saveetha.com. Mobile: +91 8072689546

Abstract

This study focuses on the eco-friendly synthesis of multifunctional nanoparticles (BE-ZnO-NPs) using betanin, a natural pigment found in beetroot, known for its antioxidant, anti-inflammatory, and antimicrobial properties. The nanoparticles were characterized using UV-visible spectroscopy, FTIR, FE-SEM, HR-TEM, EDX, XRD, DLS, and zeta potential analysis. BE-ZnO-NPs showed surface plasmon resonance at 388 nm and a hexagonal wurtzite structure, with an average particle size of 37 nm. Zinc content was determined to be 29.16% by weight. Zeta potential revealed a charge of -3.3 mV, while DLS showed a hydrodynamic diameter of 38.73 nm. The BE-ZnO-NPs demonstrated strong antibacterial activity against *E. faecalis* (18 ± 0.14 mm) and *S. mutans* (14 ± 0.18 mm) at 100 µg/mL. Antioxidant assays showed a dose-dependent scavenging effect, comparable to ascorbic acid. Cytotoxicity assays on KB cancer cells revealed an IC_{50} value of 24.29 µg/mL, indicating significant antitumor activity. qRT-PCR analysis confirmed the upregulation of pro-apoptotic genes P53 and BAX, and downregulation of BCL2, demonstrating induction of apoptosis through the intrinsic pathway. These findings underscore the potential of BE-ZnO-NPs in oral cancer treatment and as an antimicrobial agent against tooth infections.

Keywords: Betanin, ZnO-NPs, Dental pathogens, Antioxidant, KB oral cancerous cells

1. Introduction

Nanotechnology has emerged as a rapidly expanding field with diverse applications across multiple disciplines, including physics, chemistry, biology, electronics, antimicrobials, and agriculture [1]. The recent advances in nanotechnology, particularly in developing nanomaterial-based therapies, offer promising solutions for combating oral cancer and dental infections [2]. Metallic nanoparticles, such as Ag NPs, Au NPs, Se NPs, and MgO NPs, have diverse applications. Among them, zinc oxide nanoparticles (ZnO NPs) have gained considerable attention in biomedicine due to zinc's natural presence in human cells and its essential role in immune system support [3]. While ZnO NPs are widely used in the rubber industry to enhance the durability, strength, and anti-aging properties of rubber composites, they also find applications in improving the properties of polymers [4]. In addition to their industrial uses, ZnO NPs are increasingly integrated into personal care products due to their unique properties [5]. Notably, their potent antibacterial and anticancer activities have propelled their utilization in the biomedical field [6]. ZnO NPs, known for their intrinsic

antibacterial properties, are emerging as a promising approach for treating oral infections and other related health conditions [7].

The natural world offers a rich source of potential treatments for human diseases [8]. Plants contain bioactive secondary metabolites, many of which show promise as anticancer agents and have a wide range of therapeutic applications [9]. Betanin, a natural pigment predominantly found in beetroots (*Beta vulgaris*), belongs to the betalain family [10]. It is responsible for the red-violet coloration and is widely recognized for its potent antioxidant, anti-inflammatory, and chemo preventive properties [11]. Owing to its diverse biological activities, betanin has garnered significant interest in the fields of biomedicine, pharmaceuticals, and functional foods [12]. Apart from its therapeutic properties, betanin is a bio-compatible, eco-friendly compound, making it a promising candidate for green synthesis of nanoparticles [13]. Betanin acts as both a reducing and stabilizing agent during nanoparticle synthesis, leading to biocompatible ZnO nanoparticles with enhanced biological activities [14]. The synergistic effect of betanin's inherent therapeutic properties and the functional versatility of ZnO nanoparticles opens up new possibilities for applications in cancer therapy, antimicrobial treatments, and oxidative stress-related disorders [15]. BE can reduce zinc ions (Zn^{2+}) to ZnO nanoparticles under mild conditions, eliminating the need for toxic chemicals [16]. These phytochemicals not only facilitate the synthesis but also impart additional bio-functional properties to the nanoparticles. BE ZnO nanoparticles provide an advanced drug delivery system by leveraging the antioxidant and bioactive properties of betanin, along with the high surface area and biocompatibility of ZnO. This combination facilitates targeted drug delivery, enhances cellular uptake, and improves therapeutic efficacy, particularly in anticancer applications [17]. BE phytochemical-based ZnO NPs synthesis is an emerging, sustainable approach that combines the therapeutic potential of natural plant compounds with the versatile properties of ZnO nanoparticles, offering promising applications in healthcare and environmental science [18].

Oral cancer, which includes malignant tumors originating from the lips, tongue, gums, palate, and floor of the mouth, remains a significant global health concern, with nearly 300,000 new cases reported annually [19]. Despite progress in diagnostic and therapeutic interventions, the prognosis of oral cancer remains dismal, characterized by high morbidity and mortality rates [20]. Concomitantly, dental microorganisms, a diverse array of bacteria in the oral cavity, contribute to multiple oral health disorders such as dental caries, periodontal disease, and various infections [21]. Among these pathogens, *Enterococcus faecalis, Candida albicans, Streptococcus mutans*, and *Staphylococcus aureus* stand out due to their ability to colonize oral

surfaces, evade host immune responses, and cause localized as well as systemic infections [22]. *S. aureus*, a Gram-positive bacterium prevalent on the skin and nasal passages, frequently invades the oral cavity, contributing to endodontic infections, dental abscesses, and periodontal disease [23]. *S. mutans*, the leading cause of dental caries worldwide, thrives in acidic environments by metabolizing dietary carbohydrates and forming biofilms, which protect the bacterium and expedite tooth decay [24]. *C. albicans*, a polymorphic fungus, may transition from a benign commensal to a virulent pathogen, triggering oral candidiasis, an opportunistic infection characterized by white plaques on the oral mucosa [25]. *E. faecalis* is another Gram-positive bacterium commonly associated with persistent endodontic infections, capable of forming biofilms that resist antibiotics and conventional root canal treatments [26]. Oral health is intrinsically linked to systemic health, and these oral pathogens present a clinical challenge due to their resistance to standard antimicrobial therapies [27]. Concurrently, oral cancer continues to pose a serious healthcare burden, marked by its aggressive nature and limited treatment options [28]. Therefore, there is an urgent need for innovative therapeutic solutions that can simultaneously combat oral cancer and tackle infections caused by these resilient pathogens [29]. The novelty of this study lies in the functionalization of ZnO-NPs with betanin, a natural pigment derived from beets, which not only enhances the nanoparticles antimicrobial efficacy but also exhibits potent anticancer activity [30]. Betanin's ability to modulate key intracellular signalling pathways, particularly in inducing apoptosis, adds a novel dimension to its therapeutic potential [12].

The aim of present study is to 1). Synthesis of BE ZnO-NPs and characterized by UV-Vis spectroscopy, FTIR, SEM, TEM, EDX, XRD, DLS and zeta potential. 2). The synthesized BE-ZnO NPs were assessed for antibacterial efficiency against *S. aureus, S. mutans, C. albicans*, and *E. faecalis* by using well diffusion method and minimum inhibitory concentration. 3). Then BE-ZnO NPs were evaluated for antioxidant potential by DPPH and ABTS assay. 4). Additionally, In-silico molecular docking was assessed for BE against selected oral bacterial biofilms. 5). Furthermore, eco-friendly synthesized BE-ZnO were tested for KB oral cancer cells by MTT assay and its gene expression study was performed to understand the molecular mechanisms involving the BCL-2/BAX/P53 signalling pathway, which regulates cell death. The dual-functional approach not only offers a potential breakthrough in oral cancer therapy but also proposes an innovative solution for combating resistant dental pathogens, marking a significant advancement in the field of nanomedicine.

2. Materials and methods

2.1. Bio-synthesis of BE-ZnO nanoparticles

200 mg of Betanin powder is dissolved in 10 mL of double distilled water, the concentration of the Betanin solution is 20 mg/mL. After that, 40 mL of a 0.1 M zinc nitrate solution are dissolved in the betanin solution, and the mixture is continuously stirred for two hours at room temperature to create ZnO-NPs. The pH of the mixture is then adjusted to approximately 10 by adding 0.1 M NaOH solution dropwise, and the reaction is allowed to proceed for an extra 2 h to ensure completion. Following the environmentally friendly synthesis technique, plant compound based ZnO-NPs are formed more easily. The precipitate is then separated by centrifuging the NPs for 10 min at a speed of 12000 rpm. To obtain the final product, the precipitate is vacuum-dried at 60°C for 12 h after being cleaned of contaminants with distilled water.

2.2. Characterization of BE-ZnO-NPs

The BE-ZnO-NPs diffused in purified water were scrutinized over the 200–800 nm wavelength band with a UV–Vis spectrophotometer to obtain the absorption spectra, which showed the NPs' energy bandgap [31]. Using a scanning electron microscope (SEM) and TEM the shape and size distribution of the produced NPs were investigated [32]. X-ray Diffraction (XRD) examination revealed details about the NPs crystallite sizes and crystallographic phases [33]. The synthesized NPs chemical bonds and functional groups were examined using Fourier-transform infrared spectroscopy [34]. Furthermore, Energy Dispersive X-Ray Analysis (EDAX) is used for elemental analysis of nanoparticles [35]. Moreover, ZnO NPs size of particles, charge, and stability were assessed using DLS and zeta potential [36].

2.3. Antimicrobial properties

The clinical pathogenic strains of *Staphylococcus aureus* (ATCC 25923)*, Streptococcus mutans* (MTCC 890)*, Enterococcus faecalis* (MTCC 439)*,* and *Candida albicans* (MTCC 183) were obtained from the Department of Cariology, Saveetha Dental College Tamil Nadu, India. The pathogenic cultures were properly sub-cultured and maintained in our laboratory. The well diffusion method was used to assess BE-ZnO NPs antibacterial efficacy against infections in the mouth [37]. After being autoclave-sterilized for 20 min at 121°C, Mueller-Hinton agar (MHA) was transferred to a petri plate and allowed to solidify. Once spread plates were ready, 100 µL of bacterial culture (1.5 x 10^{-8} cells) were added. The broth culture that has been cultivated overnight and diluted to meet the 0.5 McFarland turbidity criterion is used for inoculation [5]. Using an industrial well puncher or a clean cork borer, drilling was made on

the agar. Various BE-ZnO-NPs concentrations (50 & 100 µg/mL) were introduced into the holes on multiple plates. As a positive control, use 5 µg/mL of Amoxicillin [38]. Following that, the plates underwent incubation for 18 to 24 h at the microorganism's ideal temperature (for example, 37°C for bacteria or 25°C for fungus). The antimicrobial activity of BE-ZnO-NPs was evaluated by looking at the plates shortly after incubation and measuring the diameter of the visible inhibition zone surrounding each well in mm with a calibrated ruler [39].

2.3.1. Minimal inhibitory concentration (MIC)

The minimal amounts of BE-ZnO NPs required to prevent the apparent spread of the oral microorganisms *S. aureus, S. mutans, E. faecalis,* and *C. albicans* was determined using the MIC assay [40]. A sterile microtiter plate containing 5, 25, 50 and 100 µg/mL of BE-ZnO-NPs at different measurements was placed in each well. Each well received an extra 100µL of inoculum, which included a standardized solution of the dentistry bacteria at a concentration of roughly 1-2 × 10^5 CFU/mL. After that, the plate was sealed and incubated for 24 h at a suitable temperature for the microbes on it (for example, 37°C for bacteria and 25°C for fungus). Following incubation, the amount of microbiological development inside each well was physically evaluated [41]. The minimum inhibitory concentration (MIC) was then calculated as the lowest concentration that totally inhibited visual growth, as shown by the lack of colonies or turbulence [42].

2.4. Antioxidant Activity

2.4.1. DPPH assay

Antioxidants' capacity to provide hydrogen atoms or electrons is taken seriously when performing the DPPH test because it helps to obtain eliminate of the DPPH radical, an unstable radical that stays and has an electron without pairing [43]. The BE-ZnO-NPs test sample's antioxidant activity was determined using the DPPH assay. To put it briefly, BE-ZnO-NPs were synthesized in four different dosages: 5, 25, 50, and 100 µg/mL. By dissolving DPPH in ethanol, the free radical became accessible in a 0.1 mM solution. After combining 100 µg/mL of BE-ZnO-NPs at various concentrations with 900 µL of DPPH solution, the mixture was incubated for thirty minutes at room temperature in darkness [44]. The absorbing capacity of the resulting liquid was measured at 517 nm using an UV-visible spectrometer [45].

2.4.2. ABTS Assay

The ABTS test assesses an antioxidant's ability to eliminate ABTS free radicals, which are created when Potassium peroxodisulfate becomes oxidized ABTS [46]. By combining potassium peroxodisulfate (2.45 mM) with the solution of ABTS (7 mM), the ABTS radicals cationic was produced [47]. The combination was then let to remain at room temperature in the dark for 16 h. After diluting the obtained ABTS solution with alcohol, the absorbance at 734 nm was found to be 0.70 ± 0.02. Different amounts of BE-ZnO-NPs were synthesized, namely 5, 25, 50, and 100 µg/mL. A portion (100 µL) of the BE-ZnO-NPs at different concentrations were mixed with 900 µL of the denatured ABTS solution, and the combination was left to kept at room temperature and in the dark for a period of 6 min. At a wavelength of 734 nm, the absorption value of the resulting liquid was measured using a spectrophotometer with an UV-Vis filter [48].

2.5. Molecular docking study

2.5.1. Selection and preparation of Proteins

The 4 dental pathogens receptor are retrieved from RCSB Protein data bank with less than or equal to 3 Å resolution [49]. The selected proteins which include Crystal structure of the N240A mutant of *Candida albicans* Mep2 (PDB ID: 6EJ6) having resolution 1.65 Å then *Enterococcal* surface protein, partial N-terminal region (PDB ID: 6ORI) with resolution 1.40 Å. Furthermore, Refined Solution Structure of Histidine Containing Phosphocarrier Protein from *Staphylococcus aureus* (PDB ID: 1KA5) and crystal structure of mutant of (Q32A) thioesterase enzyme SAV0944 from *S. mutans* Mu50 (PDB ID: 4YBV) having resolution 2.00 Å.

2.5.2. Selection of ligand

The ligand "Betanin" is selected from Pub Chem database (https://pubchem.ncbi.nlm.nih.gov/) which were retrieved as 3D SDF format having molecular formula $C_{24}H_{26}N_2O_{13}$.

2.5.3. Molecular docking

The molecular docking is performed in PyRx software the selected ligand is converted from SDF format to PDB format using Open Babel GUI software [50]. Then proteins are already in PDB format which is imported as macromolecule. Then grid box is developed in the protein in maximum level. Then docking score is predicted. The predicted docking score is compared with standard amoxicillin antibiotic [51].

2.5.4. Receptor ligand interaction

The receptor-ligand interaction refers to the interaction between a biological receptor molecule (such as a protein) and a ligand molecule (such as a drug candidate or substrate) [52]. This interaction is pivotal in understanding the mechanism of action of drugs, enzymes, and other biomolecules which is performed in Biovia Discovery studio 2021 client software [53]. The betanin interaction with dental proteins is predicted in 3D structure and in 2D structure which is saved as image files. Which expresses bond length, bond length and amino acids.

2.5.5. ADMET prediction

SwissADME predicts the Absorption, Distribution, Metabolism, Excretion, and Toxicity (ADMET) characteristics of small compounds using computer models and algorithms [54]. we have to input the chemical structure or SMILES of ligand and the tool calculates various physicochemical properties and utilizes Quantitative Structure-Activity Relationship (QSAR) models and machine learning algorithms to estimate ADMET parameters such as oral absorption, distribution in tissues, metabolic stability, clearance, and toxicity endpoints. The output includes predictions for each property along with confidence scores, assisting researchers in assessing drug-likeness and safety profiles of molecules during drug discovery and development [55].

2.6. Cytotoxicity study

The National Centre for Cell Science in Pune, India provided the KB oral cancerous cells used in this investigation. They were raised in GibcoTM DMEM with elevated glucose levels and sodium bicarbonate added as supplements. To enhance the medium, 10% fetal bovine serum (FBS), along with 100 U/mL each of streptomycin and penicillin (Sigma, St. Louis, MO, USA), was added. Cells were cultured at 37°C in a humid environment containing 5% CO_2 in an incubator made by Thermo Scientific (USA) to ensure ideal growth parameters. For each development of cells and preservation, T25 flasks which have an outer area of 25 cm^2 were used. First, 0.2×10^6 cells were planted into every flask to help with cell divisions. Beginning with 805 confluent T25 flasks, this procedure was carried out. Cells were grown in 96-well plates at 5.0×10^3 cells in each well for the purpose of the study, to ensure the right quantity of cells for the research's evaluations [56].

2.6.1. MTT assay

The KB cancer cells, were cultured in Dulbecco Modified Eagle Medium with a concentration of 10% foetal bovine serum (FBS) as well as one percent penicillin-streptomycin added. The

cultures were kept in an incubator that was humidified and contained 5% CO_2 at 37°C. Once the cells reached 70–80% confluency, varying concentrations of BE-ZnO-NPs were applied. After a 24 h exposure to BE-ZnO-NPs, the cell viability was assessed using the MTT assay. In this process, the cells were rinsed with phosphate-buffered saline (PBS) after the medium was removed. Following the addition of MTT solution (5 mg/mL in PBS) to each well, the cells underwent incubation for a further three hours at 37°C. After the incubation period, the formazan crystals were dissolved using dimethyl sulfoxide (DMSO) and the MTT solution was aspirated. The wavelength of absorption of the resulting solution was measured at 570 nm using the microplate reader.

2.6.2. Expression of the apoptotic gene

The amount of generated cDNA can be evaluated to evaluate the expression of gene and provide information on how genes are regulated in different experimental setups. Following the manufacturer's instructions, KB cells treated with BE-ZnO-NPs had their total RNA extracted using the Trizol reagent [57]. To summarize, RNA-containing water phase was extracted from cells after they were lysed using Trizol and chloroform was used [58]. Subsequently, RNA was isolated using iso-propanol, wiped with alcohol, and suspended in RNase-free liquid. Using a spectrophotometer, the amount and purity of the RNA was verified [59]. First-strand cDNA was produced for cDNA synthesis by following the manufacturer's instructions and utilizing a reverse transcription kit. RNA samples were processed with a combination of reverse transcription enzyme, randomized primers, dNTPs, and RNase blocker for one hour at 37°C. After five minutes of heating at 95°C to halt the process, the cDNA was preserved for subsequent use at -20°C. Using gene-specific primers mentioned in Table 1, quantitative RT-PCR (qRT-PCR) was performed to investigate how genes behave in BE-ZnO NPs treated KB cells. The PCR was conducted under the following conditions: 5 min of first denaturation at 95°C, forty sessions of denaturation at 95°C for thirty seconds, annealed for thirty seconds, and extension at 72°C for thirty seconds. Using the $2-\Delta\Delta Ct$ method, the mRNA levels were computed after being standardized against a domestic gene, such as GAPDH [60].

2.7. Statistical analysis

One-way ANOVA, one-sample t-tests, and Wilcoxon tests were used in the statistical evaluation to determine the significance of the differences between the control group and the different amounts of BE-ZnO-NPs. Significance was determined at levels of $*p < 0.05$, $**p <$

0.005, and ***p < 0.0005. Each experiment was performed in triplicate, and the data are presented as mean ± standard deviation.

3. Results and discussion

3.1. UV analysis

Biogenic formation of BE-ZnO nanoparticles was performed using flavonoid betanin. A shift in color from pink to brown initially confirmed the production of nanomaterials. During the synthesis of Zn nanoparticles, betanin might have functioned as stabilizing and reducing agents. Using a UV–Visible spectrophotometer, the optical attributes of ZnO nanoparticles were examined in the 300–600 nm spectrum range [31]. The present study UV/Vis spectrum revealed the highest surface plasmon resonance absorption of the synthesized BE-ZnO-NPs exhibited peak at 388 nm (pH 10) (Fig.1). Then the band energy gap was found to be 2.80 eV. This characteristic absorbance of the peak reveals the formation of ZnO-NPs. According to Hajinur Hirad et al., [14] study exhibit peak was observed at 383 and 388 nm which confirms formation of ZnO-NPs. Similarly, Habib et al., [61] demonstrated study in orange peel mediated ZnO-NPs which exhibits 367 nm UV absorbance. Likewise, Abegunde et al., [62] study shows strong excitonic UV absorption at 373 nm. Also, Segun Michel et al., [63] synthesized ZnO-NPs in *Nauclea latifolia* fruit which was observed 365 nm.

3.2. FTIR analysis

FTIR helps in characterizing the surface chemistry and confirming the presence of specific organic or inorganic components [64]. By measuring the absorption of infrared radiation at various wavelengths, FTIR can provide a detailed spectrum that indicates the vibrational modes of the chemical bonds present in ZnO-NPs [65]. For BE-ZnO-NPs, in the single bond region at 3272 cm^{-1}, a strong O-H stretching band is observed, indicating the presence of hydroxyl groups characteristic of the alcohol groups in BE. In the double bond region, the wavenumber 1627 cm^{-1} shows a strong C=O stretching band, suggesting the presence of carbonyl groups typical of δ-lactam structures found in BE. Additionally, in the fingerprint region, the wavenumbers 1147 cm^{-1} and 1076 cm^{-1} display strong C-O stretching bands, corresponding to tertiary and primary alcohols, respectively, which are part of BE molecular structure. Lastly, the wavenumber at 991 cm^{-1} indicates a strong C=C bending band, representing the alene groups within BE. These wavenumbers collectively confirm the presence and involvement of BE in the synthesis of ZnO nanoparticles, highlighting its functional groups such as hydroxyl, carbonyl, and alene groups (Fig.2B). Comparatively, the FTIR analysis of only BE reveals

different functional groups and potential impurities (Fig.2A). In the single bond region at 3333 cm^{-1}, a strong O-H stretching band is observed, indicating the presence of hydroxyl groups, likely from Betanin or its degradation products. In the fingerprint region, the wavenumbers 1352 cm^{-1} and 1015 cm^{-1} show strong C-F stretching bands, suggesting the presence of fluoro compounds, which might not be directly related to BE but could indicate impurities or specific interactions involving fluorine during the synthesis process. Additionally, the wavenumber at 335 cm^{-1} displays a strong C-Cl stretching band, indicating the presence of chloro compounds. These could be part of the initial reagents or result from interactions during the synthesis. Overall, the FTIR spectrum of BE-ZnO nanoparticles shows a clear presence of Betanin's characteristic functional groups, such as hydroxyl and carbonyl groups, as well as some impurities or interaction products, such as fluoro and chloro compounds. In contrast, the FTIR spectrum of pure Betanin mainly highlights its inherent functional groups without the additional bands associated with the synthesis process. This comparison underscores the complex chemical environment and interactions involved in the synthesis of ZnO nanoparticles mediated by BE, reflecting both the preservation of BE functional groups and the introduction of new groups or impurities during the process. Similarly, Hajinur Hirad et. al., [14] demonstrated BE ZnO NPs exhibits the Peak at 552 to 480 cm-1 confirms BE coated ZnO NPs. Since it closely correlates to the Zn–O bonds within the ZnO crystal lattice, the large peak at 569.9 cm−1 is significant. Its existence confirms that ZnO nanoparticles were successfully formed [63].

3.3. SEM and TEM analysis

The SEM study of BE-ZnO-NPs displays a variety of appearances, with the majority of the crystallized nanoparticles being less than 100 nm (Fig. 3 A & B). These NPs have a tendency to cluster together, forming irregularly shaped aggregates, likely due to strong interparticle interactions or the surface chemistry influenced by BE. Particular NPs often retain shiny exteriors with a few small imperfections despite this aggregation. Because some of the NPs show facets that might be indicative of crystal faces, the SEM pictures also point to the presence of crystalline structures. Nevertheless, additional examination employing methods such as X-ray diffraction would be required to validate the crystalline properties of the nanoparticles.

TEM provides a complementary perspective, delving deeper into the internal structure and size uniformity of the NPs. TEM imaging reveals that the BE-ZnO-NPs definitely form agglomerates, clustering into irregular shapes similar to those observed in SEM. These clusters

show a uniform particle size distribution, with particles consistently measuring around 37 nm (Fig.3 C &D). The high-resolution TEM images offer additional insights into the internal morphology and crystallinity of the NPs, further corroborating the observations made via SEM. Together, the SEM and TEM analyses offer a comprehensive understanding of the BE-ZnO-NPs complex morphology. Similarly, Mohamed Faizeea et al. [66] demonstrated that *Beta vulgaris*-mediated ZnO nanoparticles (BE-ZnO-NPs) exhibit particle agglomeration, as evidenced by TEM and SEM images, and have a spherical morphology. According to Mohammod Aminuzzaman et al., [67] reported the ZnO nanoparticles synthesized using *Hylocereus polyrhizus* are pure and exhibit a spherical shape with an average size of 56 nm. According to Johnsy Sugitha et al., [68] TEM images showed that the ZnO nanoparticles had an average size of 26 nm and were spherical in shape. Additionally, Esrat et al., [69] observed that the shape of the ZnO nanoparticles was shown by the TEM pictures, where the 50 nm & 100 nm scale bars showed an architecture similar to cotton.

3.4. Energy-dispersive X-ray spectroscopy

The EDX analysis of BE-ZnO-NPs reveals a comprehensive elemental composition, confirming the presence of Carbon (C), Nitrogen (N), Oxygen (O), and Zinc (Zn). The weight percentages for these elements are 5.99% for Carbon, 18.76% for Nitrogen, 46.08% for Oxygen, and 29.16% for Zinc. The presence of Carbon and Nitrogen is attributed to the Betanin molecules coating the ZnO nanoparticles, while the high Oxygen and Zinc content confirms the primary oxide composition of the nanoparticles (fig.4E). Elemental mapping further elucidates the distribution of these elements within the sample. Carbon and Nitrogen are uniformly dispersed, indicating a consistent coating of Betanin on the nanoparticle surface (Fig.4 A&B). Oxygen mapping highlights the oxide nature of the nanoparticles (Fig.4C), and Zinc mapping shows concentrated regions, denotes the synthesis of ZnO nanoparticles (Fig.4D). The overlay of oxygen and zinc maps reinforces the ZnO structure. These findings collectively demonstrate the successful synthesis of BE-ZnO-NPs, with the EDX and mapping data validating the effective integration of Betanin and the structural integrity of ZnO. This synthesis and coating process is crucial for the intended biological and chemical applications of these nanoparticles. According to Shah Faisal et al., [70] investigated the atomic weight of oxygen in the ZnO nanoparticles was 48.83%, while its weight percentage was 21%. Conversely, the atomic weight of zinc was 37.16%, with a weight percentage of 65.35%. The presence of other minor constituents in the ZnO nanoparticles was attributed to the root extract of ginger.

3.5. XRD analysis

One common method for figuring out a material's crystalline makeup is X-ray diffraction (XRD), which can be applied to ZnO-NPs [71]. The (100), (002), (101), (102), and (110) planes are represented by the different peaks at 2θ angles of 31.77°, 34.57°, 47.58°, 56.35°, and 67.85° that are shown by the X-ray diffraction (XRD) study of BE-ZnO-NPs. These peak values correspond with standard JCPDS card no. 36-1451 (Fig. 5) and show the hexagonal shape of the wurtzite of ZnO. The extremely crystalline nature of the produced nanoparticles is suggested by the crisp and strong diffraction peaks. In the synthesis process, betanin a naturally occurring dye present in beetroot probably serves as a cap and reducing agent. Betanin's functional groups stabilise the nanoparticles and aid in the reduction of zinc ions to ZnO, so averting clumping. The lack of FWHM values prevented the Debye-Scherrer formula from determining its crystal size, although the XRD pattern points to well-crystallized nanoparticles. Susan Azizi et al. [72] reported that the XRD results revealed the hexagonal wurtzite structure of *Citrullus colocynthis* ZnO nanoparticles. Likewise, Amal et al., [73] demonstrated the XRD pattern of nanoparticles of ZnO made using leaf extract from *Phlomis*. Two diffraction peaks, representing the (100), (002), (101), (102), (110), (103), (200), (112), (201), (004), and (202) planes, were found at 2θ = 31.8341°, 34.4911°, 36.321°, 47.6034°, 56.6643°, 62.9192°, 66.4384°, 68.0045°, 69.1421°, 72.6285°, and 77.0281°, respectively. Ehab et al. [60] reported the identification of seven unique peaks at 2θ degrees in ZnO-NPs synthesized using *Arthrospira platensis*, corresponding to the (100), (002), (101), (102), (110), (103), and (112) planes.

3.6. DLS and Zeta potential

DLS may be used to investigate a nanoparticles size, particle size distribution, and charge on its surface [74]. This technique is based on the relationship between the Brownian motion of spherical particles and light moving through the mixture of colloids [36]. Our present study BE-ZnO-NPs exhibits the polydispersity index with hydrodynamic diameter of 38.73 nm, which confirms eco-friendly synthesis of ZnO-NPs is shown in fig.6A The determination of nanoparticle dispersion, stability, and effective surface electric charge all depend on the zeta potential. In our present study BE-ZnO-NPs showed a negative charge of -3.3 mV (Fig.6B). In previous studies, Youssef et al., [75] reported that the ζ-potential analysis of *Rhus coriaria*-mediated ZnO nanoparticles showed a negative charge of -19.9 ± 0.1663 mV. Similarly,

Parthasarathi et al., [76] reported that the average size of the nanoparticles synthesized using shilajit extract was 348 nm, with a PDI of 0.322.

3.7. *In-silico* prediction BE interaction with dental pathogen and ADMET parameters

A potential connection among BE and the binding proteins of four oral bacterium which includes *C. albicans, E. faecalis, S. aureus,* and *S. mutant* was revealed by the computational docking study (Fig.7). The docking scores of betanin with various protein structures indicate its potential as a versatile ligand with varying binding affinities. For Candida albicans mutant (PDB ID: 6EJ6), a score of -6.4 suggests moderate binding, primarily involving hydrophobic interactions with nonpolar residues (MET, LEU, ILE) and potential hydrogen bonding with a serine (SER) residue, with water molecules possibly forming a hydration shell. Betanin shows a higher affinity for Enterococcal faecalis surface protein (PDB ID: 6ORI) with a score of -8.0, interacting with both polar (HIS, TYR, ASN, SER, THR) and nonpolar (VAL, GLY) residues, indicating strong hydrogen bonding and π-π stacking interactions. For Staphylococcus aureus protein (PDB ID: 1KA5), the docking score of -7.2 reflects good binding affinity, with interactions involving polar (THR, SER, LYS, GLU) and nonpolar (ILE, VAL) residues, highlighting the role of hydrogen and ionic bonds. In Staphylococcus mutant protein (PDB ID: 4YBV), a score of -7.3 suggests stable interaction primarily with glutamate (GLU) and water molecules, indicating potential hydrogen and ionic interactions stabilized by water bridges. Overall, betanin's docking scores ranging from -6.4 to -8.0 across different proteins underscore the significance of both hydrophobic and hydrophilic interactions, with hydration effects playing a role in ligand-protein stability. The binding affinity of interacted proteins with ligands and amino acid interaction were shown in (Table. 2). The *in silico* ADMET (Absorption, Distribution, Metabolism, Excretion, and Toxicity) study (Table. 3) provides a comprehensive analysis of a compound's properties, offering insights into its potential as a drug candidate. The compound betanin demonstrates low lipophilicity and poor pharmacokinetic properties, including low gastrointestinal absorption and inability to cross the blood-brain barrier. It does not inhibit major CYP enzymes or act as a Pgp substrate, which reduces the risk of drug-drug interactions. However, it violates multiple drug-likeness criteria, indicating challenges in developing it as an orally bioavailable drug. The low bioavailability score supports this conclusion. Overall, these properties suggest that while the compound may have some favourable pharmacokinetic aspects, its poor absorption and multiple drug-likeness violations may limit its potential as a drug candidate. Likewise, Siddikey et al., [77] observed the most active and common binding sites as GLY159, ASN165, and SER166 for *C. botulinum*; ASP8,

LYS40, and TRP50 for *E. coli*; and ARG37, GLN5, and ARG74 for *S. typhi*. Hosein et al. [78] found that betanin strongly inhibits TNF-α, iNOS, and NF-κB-p65 with affinities of -9.6, -9.1, and -8.5 kcal/mol, respectively. Key interacting amino acids for these sites include Val152, Pro178, and Ser177 for TNF-α; Asp289 and Arg255 for iNOS; and Asn190 and Arg274 for NF-κB-p65. Betanin also binds IL6 with an affinity of -7.3 kcal/mol, interacting with Cys76 and Arg66. These interactions suggest that betanin's anti-inflammatory effects are linked to its binding with these critical targets.

3.8. Antimicrobial activity of BE-ZnO-NPs

Many diseases in people and animals are caused by infectious bacteria and fungus [79]. To address microbial resistance and the indiscriminate use of antibiotics, extensive research and advanced scientific methods are crucial for developing new therapeutic strategies [80]. The dental pathogens evaluated in this investigation, *S. aureus, S. mutans, E. faecalis*, and *C. albicans*, were all susceptible to BE-ZnO-NPs at 50 µg/mL and consistently showed effective antibacterial action against targeted pathogen (fig. 8). This suggests that the growth of these pathogens was successfully suppressed at concentrations of 50 µg/mL and above (Fig. 9). BE-ZnO-NPs antibacterial activity was further supported by the zone of inhibition assay. For *S. aureus, S. mutans, E. faecalis*, and *C. albicans*, the inhibition zones measured 8.2 ± 0.30 mm, 7.9 ± 0.15 mm, 12.04 ± 0.17 mm, and 11.8 ± 0.13 mm at 50 µg/mL; at 100 µg/mL, they rose to 15 ± 0.11 mm, 14 ± 0.18 mm, 18 ± 0.14 mm, and 16 ± 0.15 mm, respectively (Table 2). Comparing 50 µg/mL of BE-ZnO-NPs to 5 µg/mL of amoxicillin, the positive control, the zones of inhibition were marginally smaller. But for every pathogen studied, BE-ZnO-NPs antibacterial effectiveness greatly increased at 100 µg/mL and surpassed that of amoxicillin. According to Rana et al., [81] the study, biogenic ZnO nanoparticles made from *Celosia argentea* extract were tested against four different microbial strains, two of which were gram-positive (*S. aureus* and *B. subtilis*) and the other two gram-negative (*E. coli* and *S. typhimurium*). Utilizing the agar well diffusion method, it was found that biogenic ZnO-NPs demonstrated notable antibacterial activity in comparison to chemical ZnO-NPs and the positive control, Gentamycin. The highest concentration tested for chemical ZnO-NPs was 100 µg/mL for this comparison. Several mechanisms have been proposed to explain the antibacterial activity of green ZnO nanoparticles [82]. One key mechanism involves the release of Zn^{2+} ions upon interaction with bacterial cells. The negatively charged bacterial membrane attracts these ions via Van der Waals forces, leading to membrane disruption, inhibition of cell growth, and ultimately cell death. Another mechanism is the generation of reactive oxygen

species (ROS) such as hydrogen peroxide, hydroxyl radicals, and peroxides on the surface of ZnO-NPs. These ROS induce oxidative stress by damaging the cell membrane, DNA, and proteins, which results in cell death. Additionally, direct contact between ZnO-NPs and bacterial cell membranes can alter membrane permeability, facilitating the internalization of the NPs and causing cell damage, as noted by Alghamdi et al., [81]. Additionally, Hasnain et al., [83] ZnO-NPs synthesized using *Aquilegia pubiflora* aqueous extract exhibited significant potency against *Fusarium solani* (13 ± 1.4 mm), respectively.

3.9. Minimum inhibitory concentration

The MIC of BE-ZnO-NPs was assessed against various dental pathogens including *S. aureus, S. mutans, E. faecalis, and C. albicans*. The results indicated that BE-ZnO-NPs exhibit significant antimicrobial activity, with MIC values decreasing as the concentration of nanoparticles increased. Specifically, for *S. aureus*, the MIC values ranged from 11.03 ± 0.7 µg/mL at 5 µg/mL to 39.923 ± 0.8 µg/mL at 100 µg/mL. *S. mutans* showed inhibition from 23.087 ± 0.8 µg/mL at 5 µg/mL to 54.076 ± 0.6 µg/mL at 100 µg/mL. For *E. faecalis*, the MIC values were 36.054 ± 0.7 µg/mL at 5 µg/mL and 64.99 ± 0.8 µg/mL at 100 µg/mL. Lastly, *C. albicans* demonstrated MIC values from 34.032 ± 0.9 µg/mL at 5 µg/mL to 59.6 ± 0.9 µg/mL at 100 µg/mL (Fig. 10). The study highlighted that BE-ZnO-NPs, at higher concentrations, exhibited comparable or superior antimicrobial activity to Amoxicillin (5µg/mL), underscoring their potential as an alternative to traditional antibiotics. The enhanced antimicrobial efficacy of BE-ZnO-NPs is attributed to mechanisms such as reactive oxygen species (ROS) generation, disruption of microbial cell membranes, and the release of (Zn^{2+}) ions, which interfere with microbial metabolism and enzyme functions. Additionally, the natural antioxidant properties of Betanin could contribute to the stability and effectiveness of ZnO-NPs, while the green synthesis method aligns with sustainable and environmentally friendly practices. According to Shaik et al., [84] piperine mediated ZnO-NPs demonstrated significant antimicrobial activity, particularly against *E. faecalis*. The study revealed that piperine enhances the inhibitory effects of ZnO-NPs on *E. faecalis* compared to the control, indicating the potential of piperine mediated ZnO-NPs as an effective antimicrobial agent. According to Mansab et al., [85] Because of its thin peptidoglycan layer, *E. coli* was less susceptible to produced ZnO-R NPs (9.376 ± 0.07 mm). The area of inhibition of ZnO-NPs was 10.597 ± 0.08 mm, which was considerably less than the inhibitory zones of ciprofloxacin (32.25 ± 0.12 mm) and gentamicin (22.87 ± 0.30 mm). Compared to ZnO-NPs, ZnO-R-NPs inhibitory zones versus *E. coli* and *S. aureus* were significantly smaller. According to Wangchen et al., [86] EGCG@MNPs exhibit

excellent antibacterial properties against both *E. coli* and *S. aureus*. Furthermore, Ibrahim et al., [87] reported that adding ZnO-Hesperidin to CS significantly enhanced the nanocomposites antibacterial effect against *E. coli* and *S. aureus*. The inhibition diameter of CS against *E. coli* increased from 18.3 mm to 22.3 mm with the inclusion of 6 wt% ZnO-Hesperidin. Similarly, Joo Min et al., [88] found that ZnO-gallic acid nanoparticles exhibited inhibitory effects against five bacterial strains at concentrations of 100 and 200 µg/mL. Gallic acid (GA) was utilized in this investigation at doses between 0.6 and 4.5 µg/mL, where it did not exhibit any antimicrobial activity against the bacterial strains, despite the fact that GA is known to have bactericidal activities with a MIC of 8 mg/mL for *S. aureus*.

3.10. Antioxidant activity

The findings of the DPPH experiment (Fig. 11A) show that BE-ZnO-NPs scavenge DPPH free radicals in a dose-dependent way. At doses of 5 µg/mL, 25 µg/mL, 50 µg/mL, and 100 µg/mL, the scavenging activity rises, reaching 15%, 20%, 28%, and 76%, respectively. The antioxidant property of BE-ZnO-NPs is equivalent to the amount of ascorbic acid at 100 µg/mL. Similarly, BE-ZnO-NPs have a dependent on dose scavenge effect on ABTS radicals, as demonstrated by the ABTS assay results (Fig. 11B). The proportion of ABTS that neutralizes radicals rises dramatically with increasing BE-ZnO-NPs concentrations (5 µg/mL, 25 µg/mL, 50 µg/mL, and 100 µg/mL), reaching 15%, 22%, 26%, and 75%, correspondingly. BE-ZnO-NPs have enhanced scavenging abilities against radicals of ABTS at 100 µg/mL. According to Mansab et al., [85] reported the IC_{50} value of rutin's activity in DPPH was found to be 122.27 ± 1.25 µg/mL. Similarly, Wangchen et al., [86] examined EGCG melanin nanocomposite NPs showed antioxidant activities of 67.14 ± 1.35% on DPPH and 46.99 ± 1.12% on ABTS, compared to pure EGCG, which exhibited 38.37 ± 0.67% on DPPH and 4.01 ± 0.93% on ABTS.

3.11. Anticancer activity

Oral cancer incidence is notably higher in regions such as South and Southeast Asia, where it constitutes a major health problem [89]. According to the World Health Organization (WHO), oral cancer ranks among the top ten most common cancers globally [90]. The global burden of oral cancer is expected to rise in the coming years, driven by factors such as population growth and aging, as well as increasing exposure to risk factors like tobacco use, alcohol consumption, and human papillomavirus (HPV) infection [28]. For instance, India accounts for nearly one-third of the global burden of oral cancer, with an estimated 77,000 new cases and 52,000 deaths annually [91]. In these regions, the use of smokeless tobacco products, betel quid chewing, and

poor oral hygiene are significant contributing factors. ZnO nanoparticles offer a significant advantage in cancer treatment due to their selective targeting of cancer cells [92]. The MTT assay findings, with an IC_{50} level of 24.29 µg/mL, show a strong dose-dependent lethal effect of BE-ZnO-NPs on KB cells (Fig.12E). This shows that BE-ZnO-NPs are effective at preventing these cancer cells from proliferating. A well-known anticancer medication called tamoxifen was employed as a reference for comparative analysis (Fig.12A) [93]. The performance of BE-ZnO-NPs in terms of cytotoxicity was found to be comparable to Tamoxifen, demonstrating the potential of these nanoparticles as an alternative or complementary therapy. The underlying mechanisms through which BE-ZnO-NPs exert their anticancer effects can be attributed to several interrelated pathways. Firstly, the high surface area-to-volume ratio of ZnO-NPs facilitates their cellular uptake and interaction with cellular components. Once internalized, ZnO-NPs can induce the generation of reactive oxygen species (ROS). The elevated ROS levels cause oxidative stress, leading to damage of cellular macromolecules such as lipids, proteins, and DNA [94]. This oxidative damage can trigger apoptotic pathways, leading to programmed cell death. The mitochondria, being highly susceptible to ROS, undergo membrane potential loss, release of cytochrome c, and activation of caspases, which are crucial executors of apoptosis [94]. Betanin, a natural pigment and antioxidant, enhances the biocompatibility and stability of ZnO-NPs [95]. It also contributes to the selective cytotoxicity of these nanoparticles by modulating the oxidative stress levels within the cancer cells. BE-mediated ZnO-NPs can disrupt the redox homeostasis in cancer cells more efficiently than in normal cells, thereby sparing healthy cells while targeting cancerous ones. Additionally, Betanin can interact with cellular signalling pathways that regulate cell proliferation and apoptosis. It may inhibit the NF-κB pathway, which is often associated with cell survival and proliferation, thus sensitizing cancer cells to oxidative stress and apoptotic signals. Furthermore, the interaction of ZnO-NPs with the cellular membrane proteins can lead to membrane disruption and increased permeability. This results in the leakage of intracellular contents and further promotes cell death. The nanoparticles can also interfere with the cell cycle, causing cell cycle arrest at specific checkpoints, thereby preventing the proliferation of cancer cells. The significant cell inhibition observed at higher concentrations (77.45% at 50 µg/mL and 90.36% at 100 µg/mL) underscores the potential of Betanin-mediated ZnO-NPs as a powerful anticancer agent (Fig.12 B, C &D). The correlation coefficient (R^2 = 0.9914) supports the reliability of these findings and indicates a strong dose-response relationship. When compared with Tamoxifen, BE-ZnO-NPs showed a similar degree of cytotoxicity, suggesting that these nanoparticles could serve as a viable alternative or complement to

traditional chemotherapeutic agents. The use of natural compounds like Betanin in nanoparticle synthesis also offers the advantage of reduced side effects and improved patient tolerance.

3.12. Gene expression analysis

An effective method for comprehending the molecular processes underlying ZnO-NPs biological impacts is gene transcription analysis [96]. By examining changes in gene expression profiles, we can identify specific pathways and cellular processes that are influenced by exposure to these nanoparticles [97]. This analysis helps elucidate the potential toxicological impacts, as well as beneficial therapeutic effects, of ZnO-NPs on different cell types and organisms. When KB cells subjected to BE-ZnO-NPs at 100 µg/mL were contrasted to control and cyclophosphamide-treated cells, the qRT-PCR examination showed substantial modifications in the transcript levels of major apoptotic genes (Fig. 13). These changes provide insight into the mechanisms of apoptosis induced by BE-ZnO-NPs. The expression of BCL2, an anti-apoptotic gene, was significantly downregulated in BE-ZnO-NPs treated cells (0.55 ± 0.064) compared to the control (0.893 ± 0.03), with a p-value less than 0.01. This downregulation indicates a reduction in the survival signals within the cells, promoting apoptosis. The pro-apoptotic gene BAX was significantly upregulated in BE-ZnO-NPs treated cells (1.679 ± 0.0236) compared to the control (0.895 ± 0.05), with a p-value less than 0.001. This increase in BAX expression suggests that BE-ZnO-NPs induce the intrinsic apoptotic pathway, leading to mitochondrial dysfunction and activation of the apoptotic cascade. The tumour suppressor gene P53 was significantly upregulated in BE-ZnO-NPs treated cells (1.765 ± 0.0564) compared to the control (0.891 ± 0.04), with a p-value less than 0.01. When DNA damage occurs, P53 is essential for controlling cellular arrest and apoptosis [98]. The upregulation of P53 indicates that BE-ZnO-NPs induce cellular stress, leading to apoptosis through P53-mediated pathways. The comparison with Cyclophosphamide, a known chemotherapeutic agent, further highlights the efficacy of BE-ZnO-NPs. The observed gene expression changes in BE-ZnO-NPs treated cells were comparable to or greater than those in Cyclophosphamide-treated cells, suggesting that BE-ZnO-NPs have potent anticancer activity.

4. Conclusion

This work shows that BE-ZnO-NPs present a new and efficient way to tackle issues linked to bacteria and malignancy. The successful synthesis and characterization of BE-ZnO-NPs highlight their stability, high crystallinity, and desirable physicochemical properties, including a well-defined hexagonal wurtzite structure and a negative zeta potential BE-ZnO-

NPs significant antioxidant qualities and antibacterial activity against important dentistry microorganisms such *S. aureus, S. mutans, E. faecalis,* and *C. albicans* exhibited their promise as an agent against dental pathogens. The *In-silico* analysis further supports their targeted action by showing strong interactions with pathogen receptor proteins. Moreover, BE-ZnO-NPs exhibit significant cytotoxic effects on oral cancer cells, inducing apoptosis via the BCL-2/BAX/P53 signalling pathway. This dual functionality like antibacterial and anticancer represents a significant advancement in the development of multifunctional nanoparticles. In addition to confirming the nanoparticles' ability to cause cancerous cell death, the observed overexpression of P53 and BAX and reduction of BCL2 also provides opportunities for the use of these particles in specific cancer treatment. BE-ZnO-NPs emerge as a promising candidate for integrated therapeutic strategies, offering enhanced antibacterial action and effective induction of apoptosis in oral cancer cells. Future research should focus on optimizing these nanoparticles for clinical applications and exploring their potential in other biomedical fields.

Ethics approval and consent to participate

Not applicable.

Consent for publication

Not applicable.

Availability of data and materials

This published publication contains all of the data obtained or analysed during this investigation.

CRediT authorship contribution statement

CR and MI: organised the study, carried out the tests, divided up the chemicals, examined the equipment, and composed the report. CR: conceptualization, methodology, and CK, AFA, MI performed the antibacterial experiments. Writing, editing, and reviewing for IN, SM and CR. All authors have read and agreed to the published version of the manuscript.

Declaration of competing interest

The authors declare that they have no known competing financial interests or personal relationships that could have appeared to influence the work reported in this paper.

Data availability

Data will be made available on request.

Acknowledgment

We thank Saveetha Dental College and Hospitals and Saveetha Institute of Medical and Technical Sciences (SIMATS) for carrying out the antibacterial and anticancer activity and completing the gene expression studies.

References

[1] B. Elzein, “Nano Revolution: “Tiny tech, big impact: How nanotechnology is driving SDGs progress",” *Heliyon*, vol. 10, no. 10, p. e31393, May 2024, doi: 10.1016/j.heliyon.2024.e31393.

[2] V. Jadhav, A. Roy, K. Kaur, A. K. Rai, and S. Rustagi, “Recent advances in nanomaterial-based drug delivery systems,” *Nano-Struct. Nano-Objects*, vol. 37, p. 101103, Feb. 2024, doi: 10.1016/j.nanoso.2024.101103.

[3] G. K. Prashanth *et al.*, “Zinc Oxide Nanostructures: Illuminating the Potential in Biomedical Applications: a Brief Overview,” *BioNanoScience*, vol. 14, no. 2, pp. 1876–1896, Jun. 2024, doi: 10.1007/s12668-024-01366-4.

[4] H. Gulab *et al.*, “Advancements in zinc oxide nanomaterials: Synthesis, properties, and diverse applications,” *Nano-Struct. Nano-Objects*, vol. 39, p. 101271, Sep. 2024, doi: 10.1016/j.nanoso.2024.101271.

[5] C. R. Mendes *et al.*, “Antibacterial action and target mechanisms of zinc oxide nanoparticles against bacterial pathogens,” *Sci. Rep.*, vol. 12, no. 1, p. 2658, Feb. 2022, doi: 10.1038/s41598-022-06657-y.

[6] T. C. Thounaojam, T. T. Meetei, Y. B. Devi, S. K. Panda, and H. Upadhyaya, “Zinc oxide nanoparticles (ZnO-NPs): a promising nanoparticle in renovating plant science,” *Acta Physiol. Plant.*, vol. 43, no. 10, p. 136, Oct. 2021, doi: 10.1007/s11738-021-03307-0.

[7] F. Islam *et al.*, “Exploring the Journey of Zinc Oxide Nanoparticles (ZnO-NPs) toward Biomedical Applications,” *Mater. Basel Switz.*, vol. 15, no. 6, p. 2160, Mar. 2022, doi: 10.3390/ma15062160.

[8] Y. Linhares *et al.*, “Biodiversity: the overlooked source of human health,” *Trends Mol. Med.*, vol. 29, no. 3, pp. 173–187, Mar. 2023, doi: 10.1016/j.molmed.2022.12.002.

[9] S. Patel, V. Sathyanathan, and S. D. Salaman, “Molecular mechanisms underlying cisplatin-induced nephrotoxicity and the potential ameliorative effects of essential oils: A comprehensive review,” *Tissue Cell*, vol. 88, p. 102377, Jun. 2024, doi: 10.1016/j.tice.2024.102377.

[10] I. Sadowska-Bartosz and G. Bartosz, “Biological Properties and Applications of Betalains,” *Mol. Basel Switz.*, vol. 26, no. 9, p. 2520, Apr. 2021, doi: 10.3390/molecules26092520.

[11] B. Thippeswamy *et al.*, “Chemical Additives for Preserving the Betalain Pigment and Antioxidant Activity of Red Beetroot,” *Sugar Tech*, vol. 24, no. 3, pp. 890–899, Jun. 2022, doi: 10.1007/s12355-021-01104-0.

[12] N. P. Nirmal *et al.*, “Betalains protect various body organs through antioxidant and anti-inflammatory pathways,” *Food Sci. Hum. Wellness*, vol. 13, no. 3, pp. 1109–1117, May 2024, doi: 10.26599/FSHW.2022.9250093.

[13] A. I. Osman *et al.*, “Synthesis of green nanoparticles for energy, biomedical, environmental, agricultural, and food applications: A review,” *Environ. Chem. Lett.*, vol. 22, no. 2, pp. 841–887, Apr. 2024, doi: 10.1007/s10311-023-01682-3.

[14] A. Hajinur Hirad, A. A. Alarfaj, B. Ravindran, and S. Perumal Narasimhamoorthi, “Synthesis of Betanin Inspired Zinc Oxide Nanoparticles and to Evaluate its Anti-Oxidant and Anti-Cancer Activity,” 2023. doi: 10.2139/ssrn.4583724.

[15] D. V. T. D. Silva, D. D. S. Baião, V. F. Ferreira, and V. M. F. Paschoalin, “Betanin as a multipath oxidative stress and inflammation modulator: a beetroot pigment with protective effects on cardiovascular disease pathogenesis,” *Crit. Rev. Food Sci. Nutr.*, vol. 62, no. 2, pp. 539–554, Jan. 2022, doi: 10.1080/10408398.2020.1822277.

[16] S. Amjadi, M. Nazari, S. A. Alizadeh, and H. Hamishehkar, “Multifunctional betanin nanoliposomes-incorporated gelatin/chitosan nanofiber/ZnO nanoparticles nanocomposite film for fresh beef preservation,” *Meat Sci.*, vol. 167, p. 108161, Sep. 2020, doi: 10.1016/j.meatsci.2020.108161.

[17] M. Carofiglio, S. Barui, V. Cauda, and M. Laurenti, “Doped Zinc Oxide Nanoparticles: Synthesis, Characterization and Potential Use in Nanomedicine,” *Appl. Sci.*, vol. 10, no. 15, p. 5194, Jul. 2020, doi: 10.3390/app10155194.

[18] N. Rani, P. Singh, S. Kumar, P. Kumar, V. Bhankar, and K. Kumar, “Plant-mediated synthesis of nanoparticles and their applications: A review,” *Mater. Res. Bull.*, vol. 163, p. 112233, Jul. 2023, doi: 10.1016/j.materresbull.2023.112233.

[19] C. Watters, S. Brar, and T. Pepper, “Cancer of the Oral Mucosa,” in *StatPearls*, Treasure Island (FL): StatPearls Publishing, 2024. Accessed: Aug. 07, 2024. [Online]. Available: http://www.ncbi.nlm.nih.gov/books/NBK565867/

[20] T. I. Budhy *et al.*, “Potential of Moringa Leaf Nanoparticles (Moringa oleifera) on the Expression of TNFα, IL10, and HSP 27 in Oral Cavity Cancer,” *J. Multidiscip. Appl. Nat. Sci.*, vol. 4, no. 1, pp. 120–129, Nov. 2023, doi: 10.47352/jmans.2774-3047.198.

[21] W. J. Loesche, “Microbiology of Dental Decay and Periodontal Disease,” in *Medical Microbiology*, 4th ed., S. Baron, Ed., Galveston (TX): University of Texas Medical Branch at Galveston, 1996. Accessed: Apr. 22, 2024. [Online]. Available: http://www.ncbi.nlm.nih.gov/books/NBK8259/

[22] N. Zaatout, “Presence of non-oral bacteria in the oral cavity,” *Arch. Microbiol.*, vol. 203, no. 6, pp. 2747–2760, Aug. 2021, doi: 10.1007/s00203-021-02300-y.

[23] G. Y. C. Cheung, J. S. Bae, and M. Otto, “Pathogenicity and virulence of Staphylococcus aureus,” *Virulence*, vol. 12, no. 1, pp. 547–569, Dec. 2021, doi: 10.1080/21505594.2021.1878688.

[24] S.-C. Luo *et al.*, “How probiotics, prebiotics, synbiotics, and postbiotics prevent dental caries: an oral microbiota perspective,” *Npj Biofilms Microbiomes*, vol. 10, no. 1, p. 14, Feb. 2024, doi: 10.1038/s41522-024-00488-7.

[25] J. P. Lopes and M. S. Lionakis, “Pathogenesis and virulence of *Candida albicans*,” *Virulence*, vol. 13, no. 1, pp. 89–121, Dec. 2022, doi: 10.1080/21505594.2021.2019950.

[26] J. Wong, D. Manoil, P. Näsman, G. N. Belibasakis, and P. Neelakantan, “Microbiological Aspects of Root Canal Infections and Disinfection Strategies: An Update Review on the Current Knowledge and Challenges,” *Front. Oral Health*, vol. 2, p. 672887, 2021, doi: 10.3389/froh.2021.672887.

[27] J. J. Rajasekaran *et al.*, “Oral Microbiome: A Review of Its Impact on Oral and Systemic Health,” *Microorganisms*, vol. 12, no. 9, p. 1797, Aug. 2024, doi: 10.3390/microorganisms12091797.

[28] R. Sun *et al.*, “Global, regional, and national burden of oral cancer and its attributable risk factors from 1990 to 2019,” *Cancer Med.*, vol. 12, no. 12, pp. 13811–13820, Jun. 2023, doi: 10.1002/cam4.6025.

[29] H. Alaoui Mdarhri *et al.*, “Alternatives Therapeutic Approaches to Conventional Antibiotics: Advantages, Limitations and Potential Application in Medicine,” *Antibiot. Basel Switz.*, vol. 11, no. 12, p. 1826, Dec. 2022, doi: 10.3390/antibiotics11121826.

[30] A. S. Alameen, S. B. Undre, and P. B. Undre, “Functionalization of ZnO nanoparticles and their antimicrobial activity: In vitro,” *Nano-Struct. Nano-Objects*, vol. 39, p. 101314, Sep. 2024, doi: 10.1016/j.nanoso.2024.101314.

[31] S. Singh, J. V. Gade, D. K. Verma, B. Elyor, and B. Jain, “Exploring ZnO nanoparticles: UV–visible analysis and different size estimation methods,” *Opt. Mater.*, vol. 152, p. 115422, Jun. 2024, doi: 10.1016/j.optmat.2024.115422.

[32] A. E. Vladár and V.-D. Hodoroaba, “Characterization of nanoparticles by scanning electron microscopy,” in *Characterization of Nanoparticles*, Elsevier, 2020, pp. 7–27. doi: 10.1016/B978-0-12-814182-3.00002-X.
[33] J. A. Kaduk *et al.*, “Powder diffraction,” *Nat. Rev. Methods Primer*, vol. 1, no. 1, p. 77, Nov. 2021, doi: 10.1038/s43586-021-00074-7.
[34] K. A. Nxumalo, J. O. Adeyemi, T. B. Leta, T. M. Pfukwa, S. N. Okafor, and O. A. Fawole, “Antifungal properties and molecular docking of ZnO NPs mediated using medicinal plant extracts,” *Sci. Rep.*, vol. 14, no. 1, p. 18071, Aug. 2024, doi: 10.1038/s41598-024-68979-3.
[35] V.-D. Hodoroaba, “Energy-dispersive X-ray spectroscopy (EDS),” in *Characterization of Nanoparticles*, Elsevier, 2020, pp. 397–417. doi: 10.1016/B978-0-12-814182-3.00021-3.
[36] M. K. Rasmussen, J. N. Pedersen, and R. Marie, “Size and surface charge characterization of nanoparticles with a salt gradient,” *Nat. Commun.*, vol. 11, no. 1, p. 2337, May 2020, doi: 10.1038/s41467-020-15889-3.
[37] A. A. El-Fallal, R. A. Elfayoumy, and M. M. El-Zahed, “Antibacterial activity of biosynthesized zinc oxide nanoparticles using Kombucha extract,” *SN Appl. Sci.*, vol. 5, no. 12, p. 332, Dec. 2023, doi: 10.1007/s42452-023-05546-x.
[38] A. R. Mendes, C. M. Granadeiro, A. Leite, E. Pereira, P. Teixeira, and F. Poças, “Optimizing Antimicrobial Efficacy: Investigating the Impact of Zinc Oxide Nanoparticle Shape and Size,” *Nanomaterials*, vol. 14, no. 7, p. 638, Apr. 2024, doi: 10.3390/nano14070638.
[39] A. S. Bhosale, K. K. Abitkar, P. S. Sadalage, K. D. Pawar, and K. M. Garadkar, “Photocatalytic and antibacterial activities of ZnO nanoparticles synthesized by chemical method,” *J. Mater. Sci. Mater. Electron.*, vol. 32, no. 15, pp. 20510–20524, Aug. 2021, doi: 10.1007/s10854-021-06563-5.
[40] Z. Gao *et al.*, “New strategies and mechanisms for targeting Streptococcus mutans biofilm formation to prevent dental caries: A review,” *Microbiol. Res.*, vol. 278, p. 127526, Jan. 2024, doi: 10.1016/j.micres.2023.127526.
[41] B. Shobha *et al.*, “Trichoderma-Mediated ZnO Nanoparticles and Their Antibiofilm and Antibacterial Activities,” *J. Fungi*, vol. 9, no. 2, p. 133, Jan. 2023, doi: 10.3390/jof9020133.
[42] I. Ahmad *et al.*, “Zinc oxide nanoparticle: An effective antibacterial agent against pathogenic bacterial isolates,” *J. King Saud Univ. - Sci.*, vol. 34, no. 5, p. 102110, Jul. 2022, doi: 10.1016/j.jksus.2022.102110.
[43] R. Kumar, D. Shikha, and S. K. Sinha, “DPPH radical scavenging assay: A tool for evaluating antioxidant activity in 3 % cobalt – Doped hydroxyapatite for orthopaedic implants,” *Ceram. Int.*, vol. 50, no. 8, pp. 13967–13973, Apr. 2024, doi: 10.1016/j.ceramint.2024.01.314.
[44] S. Baliyan *et al.*, “Determination of Antioxidants by DPPH Radical Scavenging Activity and Quantitative Phytochemical Analysis of Ficus religiosa,” *Molecules*, vol. 27, no. 4, p. 1326, Feb. 2022, doi: 10.3390/molecules27041326.
[45] M. Yamauchi, Y. Kitamura, H. Nagano, J. Kawatsu, and H. Gotoh, “DPPH Measurements and Structure—Activity Relationship Studies on the Antioxidant Capacity of Phenols,” *Antioxidants*, vol. 13, no. 3, p. 309, Mar. 2024, doi: 10.3390/antiox13030309.
[46] A. Cano, A. B. Maestre, J. Hernández-Ruiz, and M. B. Arnao, “ABTS/TAC Methodology: Main Milestones and Recent Applications,” *Processes*, vol. 11, no. 1, p. 185, Jan. 2023, doi: 10.3390/pr11010185.
[47] N. Bibi Sadeer, D. Montesano, S. Albrizio, G. Zengin, and M. F. Mahomoodally, “The Versatility of Antioxidant Assays in Food Science and Safety—Chemistry, Applications, Strengths, and Limitations,” *Antioxidants*, vol. 9, no. 8, p. 709, Aug. 2020, doi: 10.3390/antiox9080709.
[48] K. Matsumoto *et al.*, “Redox reactions between ABTS•+ and dihydroxybenzenes as studied by cyclic voltammetry,” *Anal. Sci.*, vol. 38, no. 1, pp. 227–230, Jan. 2022, doi: 10.2116/analsci.21N030.

[49] D. S. Goodsell and S. K. Burley, “RCSB Protein Data Bank resources for structure-facilitated design of mRNA vaccines for existing and emerging viral pathogens,” *Structure*, vol. 30, no. 1, pp. 55-68.e2, Jan. 2022, doi: 10.1016/j.str.2021.10.008.

[50] S. K. Kondapuram, S. Sarvagalla, and M. S. Coumar, “Docking-Based Virtual Screening Using PyRx Tool: Autophagy Target Vps34 as a Case Study,” in *Molecular Docking for Computer-Aided Drug Design*, Elsevier, 2021, pp. 463–477. doi: 10.1016/B978-0-12-822312-3.00019-9.

[51] H. Chio, E. E. Guest, J. L. Hobman, T. Dottorini, J. D. Hirst, and D. J. Stekel, “Predicting bioactivity of antibiotic metabolites by molecular docking and dynamics,” *J. Mol. Graph. Model.*, vol. 123, p. 108508, Sep. 2023, doi: 10.1016/j.jmgm.2023.108508.

[52] W. Lu *et al.*, “DynamicBind: predicting ligand-specific protein-ligand complex structure with a deep equivariant generative model,” *Nat. Commun.*, vol. 15, no. 1, p. 1071, Feb. 2024, doi: 10.1038/s41467-024-45461-2.

[53] L. Sun *et al.*, “Pharmacokinetic and Pharmacodynamic Drug–Drug Interactions: Research Methods and Applications,” *Metabolites*, vol. 13, no. 8, p. 897, Jul. 2023, doi: 10.3390/metabo13080897.

[54] P. Sucharitha, K. Ramesh Reddy, S. V. Satyanarayana, and T. Garg, “Absorption, distribution, metabolism, excretion, and toxicity assessment of drugs using computational tools,” in *Computational Approaches for Novel Therapeutic and Diagnostic Designing to Mitigate SARS-CoV-2 Infection*, Elsevier, 2022, pp. 335–355. doi: 10.1016/B978-0-323-91172-6.00012-1.

[55] C.-Y. Jia, J.-Y. Li, G.-F. Hao, and G.-F. Yang, “A drug-likeness toolbox facilitates ADMET study in drug discovery,” *Drug Discov. Today*, vol. 25, no. 1, pp. 248–258, Jan. 2020, doi: 10.1016/j.drudis.2019.10.014.

[56] Senior Lecturer, Faculty of Medicine, Bioscience and Nursing, School of Bioscience, Mahsa University, Saujana Putra Campus, Jalan SP2, Bandar Saujana Putra, 42610, Jenjarom, Selangor, Malaysia and P. Iyappan, “Fucoxanthin induced apoptotic cell death in oral squamous carcinoma (KB) cells,” *Bioinformation*, vol. 17, no. 1, pp. 181–191, Jan. 2021, doi: 10.6026/97320630017181.

[57] Y.-M. Lee, H. Cho, R.-O. Kim, S. In, S.-J. Kim, and E.-J. Won, “Validation of reference genes for quantitative real-time PCR in chemical exposed and at different age’s brackish water flea Diaphanosoma celebensis,” *Sci. Rep.*, vol. 11, no. 1, p. 23691, Dec. 2021, doi: 10.1038/s41598-021-03098-x.

[58] A. Das, D. Das, and A. C. Panda, “Validation of gene expression by quantitative PCR,” in *Rigor and Reproducibility in Genetics and Genomics*, Elsevier, 2024, pp. 247–257. doi: 10.1016/B978-0-12-817218-6.00017-6.

[59] Y. Rozevsky *et al.*, “Quantification of mRNA Expression Using Single-Molecule Nanopore Sensing,” *ACS Nano*, vol. 14, no. 10, pp. 13964–13974, Oct. 2020, doi: 10.1021/acsnano.0c06375.

[60] J. Libus and H. Štorchová, “Quantification of cDNA generated by reverse transcription of total RNA provides a simple alternative tool for quantitative RT-PCR normalization,” *BioTechniques*, vol. 41, no. 2, pp. 156–164, Aug. 2006, doi: 10.2144/000112232.

[61] A. K. M. A. Habib, K. M. R. Rifat, M. E. Kabir, J. N. Khan, S. M. N. Rokon, and M. A. Rabbi, “Improved photocatalytic activity of (Ni, Mn) co-doped ZnO nanoparticles prepared via green synthesis route using orange peel extract,” *Results Mater.*, vol. 22, p. 100581, Jun. 2024, doi: 10.1016/j.rinma.2024.100581.

[62] S. M. Abegunde, M. A. Adebayo, and E. F. Olasehinde, “Green synthesis of ZnO nanoparticles and its application for methyl green dye adsorption,” *Green Energy Resour.*, vol. 2, no. 2, p. 100073, Jun. 2024, doi: 10.1016/j.gerr.2024.100073.

[63] S. M. Abegunde, E. F. Olasehinde, and M. A. Adebayo, “Green synthesis of ZnO nanoparticles using Nauclea latifolia fruit extract for adsorption of Congo red,” *Hybrid Adv.*, vol. 5, p. 100164, Apr. 2024, doi: 10.1016/j.hybadv.2024.100164.

[64] L. Mester, A. A. Govyadinov, S. Chen, M. Goikoetxea, and R. Hillenbrand, “Subsurface chemical nanoidentification by nano-FTIR spectroscopy,” *Nat. Commun.*, vol. 11, no. 1, p. 3359, Jul. 2020, doi: 10.1038/s41467-020-17034-6.

[65] C. N. Andoh, F. Attiogbe, N. O. Bonsu Ackerson, M. Antwi, and K. Adu-Boahen, “Fourier Transform Infrared Spectroscopy: An analytical technique for microplastic identification and quantification,” *Infrared Phys. Technol.*, vol. 136, p. 105070, Jan. 2024, doi: 10.1016/j.infrared.2023.105070.

[66] N. Mohamed Faizee, C. Joel, R. Imran Khan, and M. S. M. Badhusha, “*Beta vulgaris* extract assisted green synthesis of ZnO nanoparticles: antimicrobial and nano priming studies,” *Inorg. Nano-Met. Chem.*, pp. 1–10, Aug. 2023, doi: 10.1080/24701556.2023.2240759.

[67] M. Aminuzzaman, P. S. Ng, W.-S. Goh, S. Ogawa, and A. Watanabe, “Value-adding to dragon fruit (*Hylocereus polyrhizus*) peel biowaste: green synthesis of ZnO nanoparticles and their characterization,” *Inorg. Nano-Met. Chem.*, vol. 49, no. 11, pp. 401–411, Nov. 2019, doi: 10.1080/24701556.2019.1661464.

[68] S. K. J. Sugitha, R. Venkatesan, R. G. Latha, A. A. Vetcher, B. A. Al-Asbahi, and S.-C. Kim, “A Study on the Antibacterial, Antispasmodic, Antipyretic, and Anti-Inflammatory Activity of ZnO Nanoparticles Using Leaf Extract from Jasminum sambac (L. Aiton),” *Molecules*, vol. 29, no. 7, p. 1464, Mar. 2024, doi: 10.3390/molecules29071464.

[69] E. J. Rupa *et al.*, “Cissus antractica-ZnO NPs Induce Apoptosis in A549 Cells through ROS-Generated p53/Bcl-2/Bax Signaling Pathways and Inhibition of Inflammatory Cytokines,” *Coatings*, vol. 13, no. 12, p. 2077, Dec. 2023, doi: 10.3390/coatings13122077.

[70] S. Faisal *et al.*, “Green Synthesis of Zinc Oxide (ZnO) Nanoparticles Using Aqueous Fruit Extracts of *Myristica fragrans* : Their Characterizations and Biological and Environmental Applications,” *ACS Omega*, vol. 6, no. 14, pp. 9709–9722, Apr. 2021, doi: 10.1021/acsomega.1c00310.

[71] C. Marcos, “Methods and Applications of X-ray Diffraction in Crystallography and Mineralogy,” in *Crystallography*, in Springer Textbooks in Earth Sciences, Geography and Environment. , Cham: Springer Nature Switzerland, 2022, pp. 383–436. doi: 10.1007/978-3-030-96783-3_17.

[72] S. Azizi, R. Mohamad, and M. Mahdavi Shahri, “Green Microwave-Assisted Combustion Synthesis of Zinc Oxide Nanoparticles with Citrullus colocynthis (L.) Schrad: Characterization and Biomedical Applications,” *Molecules*, vol. 22, no. 2, p. 301, Feb. 2017, doi: 10.3390/molecules22020301.

[73] A. A. Alyamani, S. Albukhaty, S. Aloufi, F. A. AlMalki, H. Al-Karagoly, and G. M. Sulaiman, “Green Fabrication of Zinc Oxide Nanoparticles Using Phlomis Leaf Extract: Characterization and In Vitro Evaluation of Cytotoxicity and Antibacterial Properties,” *Molecules*, vol. 26, no. 20, p. 6140, Oct. 2021, doi: 10.3390/molecules26206140.

[74] Z. Jia, J. Li, L. Gao, D. Yang, and A. Kanaev, “Dynamic Light Scattering: A Powerful Tool for In Situ Nanoparticle Sizing,” *Colloids Interfaces*, vol. 7, no. 1, p. 15, Feb. 2023, doi: 10.3390/colloids7010015.

[75] Y. Mongy and T. Shalaby, “Green synthesis of zinc oxide nanoparticles using Rhus coriaria extract and their anticancer activity against triple-negative breast cancer cells,” *Sci. Rep.*, vol. 14, no. 1, p. 13470, Jun. 2024, doi: 10.1038/s41598-024-63258-7.

[76] P. Perumal *et al.*, “Green synthesis of zinc oxide nanoparticles using aqueous extract of shilajit and their anticancer activity against HeLa cells,” *Sci. Rep.*, vol. 14, no. 1, p. 2204, Jan. 2024, doi: 10.1038/s41598-024-52217-x.

[77] F. Siddikey, M. A. H. Roni, A. Kumer, U. Chakma, and M. M. Matin, “Computational investigation of Betalain derivatives as natural inhibitor against food borne bacteria,” *Curr. Chem. Lett.*, vol. 11, no. 3, pp. 309–320, 2022, doi: 10.5267/j.ccl.2022.3.003.

[78] H. Ahmadi, Z. Nayeri, Z. Minuchehr, F. Sabouni, and M. Mohammadi, “Betanin purification from red beetroots and evaluation of its anti-oxidant and anti-inflammatory activity on LPS-activated microglial cells,” *PLOS ONE*, vol. 15, no. 5, p. e0233088, May 2020, doi: 10.1371/journal.pone.0233088.

[79] S. R. Prabhu, “Infectious and Communicable Diseases: An Overview,” in *Textbook of General Pathology for Dental Students*, Cham: Springer Nature Switzerland, 2023, pp. 63–72. doi: 10.1007/978-3-031-31244-1_9.

[80] J. Soni, S. Sinha, and R. Pandey, “Understanding bacterial pathogenicity: a closer look at the journey of harmful microbes,” *Front. Microbiol.*, vol. 15, p. 1370818, Feb. 2024, doi: 10.3389/fmicb.2024.1370818.

[81] R. A. Alghamdi *et al.*, “Biogenic Zinc oxide nanoparticles from Celosia argentea: toward improved antioxidant, antibacterial, and anticancer activities,” *Front. Bioeng. Biotechnol.*, vol. 11, p. 1283898, Dec. 2023, doi: 10.3389/fbioe.2023.1283898.

[82] S. C. E. González *et al.*, “Antibacterial and anticancer activity of ZnO with different morphologies: a comparative study,” *3 Biotech*, vol. 11, no. 2, p. 68, Feb. 2021, doi: 10.1007/s13205-020-02611-9.

[83] H. Jan *et al.*, “Biogenic Synthesis and Characterization of Antimicrobial and Antiparasitic Zinc Oxide (ZnO) Nanoparticles Using Aqueous Extracts of the Himalayan Columbine (Aquilegia pubiflora),” *Front. Mater.*, vol. 7, p. 249, Aug. 2020, doi: 10.3389/fmats.2020.00249.

[84] M. R. Shaik *et al.*, “Piperine-coated zinc oxide nanoparticles target biofilms and induce oral cancer apoptosis via BCl-2/BAX/P53 pathway,” *BMC Oral Health*, vol. 24, no. 1, p. 715, Jun. 2024, doi: 10.1186/s12903-024-04399-z.

[85] M. A. Saleemi, B. Alallam, Y. K. Yong, and V. Lim, “Synthesis of Zinc Oxide Nanoparticles with Bioflavonoid Rutin: Characterisation, Antioxidant and Antimicrobial Activities and In Vivo Cytotoxic Effects on Artemia Nauplii,” *Antioxidants*, vol. 11, no. 10, p. 1853, Sep. 2022, doi: 10.3390/antiox11101853.

[86] W. Zhao *et al.*, “Preparation and characterization of epigallocatechin-3-gallate loaded melanin nanocomposite (EGCG @MNPs) for improved thermal stability, antioxidant and antibacterial activity,” *LWT*, vol. 154, p. 112599, Jan. 2022, doi: 10.1016/j.lwt.2021.112599.

[87] I. Erol, Ö. Hazman, M. Aksu, and E. Bulut, “Synergistic effect of ZnO nanoparticles and hesperidin on the antibacterial properties of chitosan,” *J. Biomater. Sci. Polym. Ed.*, vol. 33, no. 15, pp. 1973–1997, Oct. 2022, doi: 10.1080/09205063.2022.2099668.

[88] J. Lee, K.-H. Choi, J. Min, H.-J. Kim, J.-P. Jee, and B. J. Park, “Functionalized ZnO Nanoparticles with Gallic Acid for Antioxidant and Antibacterial Activity against Methicillin-Resistant S. aureus,” *Nanomaterials*, vol. 7, no. 11, p. 365, Nov. 2017, doi: 10.3390/nano7110365.

[89] S. V. Krishna Rao, G. Mejia, K. Roberts-Thomson, and R. Logan, “Epidemiology of oral cancer in Asia in the past decade--an update (2000-2012),” *Asian Pac. J. Cancer Prev. APJCP*, vol. 14, no. 10, pp. 5567–5577, 2013, doi: 10.7314/apjcp.2013.14.10.5567.

[90] N. Jain, U. Dutt, I. Radenkov, and S. Jain, “WHO ’s global oral health status report 2022: Actions, discussion and implementation,” *Oral Dis.*, p. odi.14516, Feb. 2023, doi: 10.1111/odi.14516.

[91] V. Borse, A. N. Konwar, and P. Buragohain, “Oral cancer diagnosis and perspectives in India,” *Sens. Int.*, vol. 1, p. 100046, 2020, doi: 10.1016/j.sintl.2020.100046.

[92] G. Bisht and S. Rayamajhi, “ZnO Nanoparticles: A Promising Anticancer Agent,” *Nanobiomedicine*, vol. 3, p. 9, Jan. 2016, doi: 10.5772/63437.

[93] Shagufta and I. Ahmad, “Tamoxifen a pioneering drug: An update on the therapeutic potential of tamoxifen derivatives,” *Eur. J. Med. Chem.*, vol. 143, pp. 515–531, Jan. 2018, doi: 10.1016/j.ejmech.2017.11.056.

[94] S. Roy Choudhury, J. Ordaz, C.-L. Lo, N. P. Damayanti, F. Zhou, and J. Irudayaraj, “ZnO nanoparticles induced reactive oxygen species promotes multimodal cyto- and epigenetic toxicity,” *Toxicol. Sci.*, p. kfw252, Jan. 2017, doi: 10.1093/toxsci/kfw252.

[95] D. Vieira Teixeira Da Silva *et al.*, “Betanin, a Natural Food Additive: Stability, Bioavailability, Antioxidant and Preservative Ability Assessments,” *Molecules*, vol. 24, no. 3, p. 458, Jan. 2019, doi: 10.3390/molecules24030458.

[96] M. A. C. Horta *et al.*, “Transcriptomic analysis of genes: expression and regulation,” in *Transcriptome Profiling*, Elsevier, 2023, pp. 1–41. doi: 10.1016/B978-0-323-91810-7.00017-0.

[97] A. Siavoshi, M. Taghizadeh, E. Dookhe, and M. Piran, “Gene expression profiles and pathway enrichment analysis to identification of differentially expressed gene and signaling pathways in epithelial ovarian cancer based on high-throughput RNA-seq data,” *Genomics*, vol. 114, no. 1, pp. 161–170, Jan. 2022, doi: 10.1016/j.ygeno.2021.11.031.

[98] B. J. Aubrey, G. L. Kelly, A. Janic, M. J. Herold, and A. Strasser, “How does p53 induce apoptosis and how does this relate to p53-mediated tumour suppression?,” *Cell Death Differ.*, vol. 25, no. 1, pp. 104–113, Jan. 2018, doi: 10.1038/cdd.2017.169.